2-27-2019

Review of Fe-6.5 wt%Si high silicon steel—A promising soft magnetic material for sub-kHz application

Gaoyuan Ouyang
Iowa State University and Ames Laboratory, gaoyuan@iastate.edu

Xi Chen
Ames Laboratory

Yongfeng Liang
Ames Laboratory

Chad Macziewski
Ames Laboratory, chadm@iastate.edu

Jun Cui
Iowa State University and Ames Laboratory, cuijun@iastate.edu

Review of Fe-6.5 wt%Si high silicon steel—A promising soft magnetic material for sub-kHz application

Abstract
To meet the growing need for energy efficiency in power electronics and electric machines, a number of new soft magnetic materials are being investigated. Among them, high silicon Fe-Si alloy has been recognized as a promising candidate for low-to-medium-frequency applications. Compared to the currently most widely used 3 wt% silicon steel, the steel containing 6.5 wt% Si possesses more favorable properties, including high electrical resistivity, good saturation magnetization, and near-zero magnetostriction. However, the high silicon content facilitates the formation of ordered phases, resulting in severe brittleness that prohibits mass production using the economical conventional processing methods. A number of new processing routes have been investigated and inspiring progress has been made. Prototypes of motors and transformers using high silicon steel have been demonstrated with improved efficiency and power density. If the processing cost and limitations of size and shape are properly addressed, high silicon steel is expected to be widely adopted by the industries. Among all the investigated processing techniques, rapid solidification appears to be the most cost-effective method for mass producing thin sheet of high silicon steel. This paper reviews the current state-of-the-art of the Fe-Si based soft magnetic materials including their history, structure, properties, processing, and applications.

Keywords
Soft magnetic material, Silicon steel, Fe-6.5 wt%Si, Processing, Magnetic properties, Physical properties

Disciplines
Materials Science and Engineering | Metallurgy

Journal of Magnetism and Magnetic Materials 481 (2019) 234–250

Contents lists available at ScienceDirect

Journal of Magnetism and Magnetic Materials

journal homepage: www.elsevier.com/locate/jmmm

Review of Fe-6.5 wt%Si high silicon steel—A promising soft magnetic material for sub-kHz application

Gaoyuan Ouyang[a,b,*], Xi Chen[a], Yongfeng Liang[a], Chad Macziewski[a], Jun Cui[a,b]

[a] Department of Material Science and Engineering, Iowa State University, Ames, IA 50011, United States
[b] Division of Materials Science and Engineering, Ames Laboratory, Ames, IA 50011, United States

ARTICLE INFO

Keywords:
Soft magnetic material
Silicon steel
Fe-6.5 wt%Si
Processing
Magnetic properties
Physical properties

ABSTRACT

To meet the growing need for energy efficiency in power electronics and electric machines, a number of new soft magnetic materials are being investigated. Among them, high silicon Fe-Si alloy has been recognized as a promising candidate for low-to-medium-frequency applications. Compared to the currently most widely used 3 wt% silicon steel, the steel containing 6.5 wt% Si possesses more favorable properties, including high electrical resistivity, good saturation magnetization, and near-zero magnetostriction. However, the high silicon content facilitates the formation of ordered phases, resulting in severe brittleness that prohibits mass production using the economical conventional processing methods. A number of new processing routes have been investigated and inspiring progress has been made. Prototypes of motors and transformers using high silicon steel have been demonstrated with improved efficiency and power density. If the processing cost and limitations of size and shape are properly addressed, high silicon steel is expected to be widely adopted by the industries. Among all the investigated processing techniques, rapid solidification appears to be the most cost-effective method for mass producing thin sheet of high silicon steel. This paper reviews the current state-of-the-art of the Fe-Si based soft magnetic materials including their history, structure, properties, processing, and applications.

1. Introduction

Soft magnetic materials are the materials that can rapidly switch their magnetic polarization under a small applied field. They are usually characterized by an intrinsic coercivity of less than 1000 A/m. Soft magnetic materials are used for power generation, condition, transfer, and conversion, and are extensively used in electric machines, power electronics, sensors, and electromagnetic interference (EMI) preventions. They play a vital role in today's energy-use sectors of the economy.

Soft magnetic materials are used in both DC and AC applications. In DC applications, a desired magnetic flux is generated when the soft magnetic materials are energized with an externally applied field, which is normally created by passing an electric current through an excitation coil. After the work is complete, the soft magnetic materials are demagnetized by removing the external field, i.e., by switching off the current in the excitation coil. Examples of typical DC applications are lifting electromagnets or electromagnetic switches. Permeability, magnetic flux density, and intrinsic coercivity are the key figures of merit in DC applications. In AC applications, the soft magnetic materials are magnetized and demagnetized repeatedly following the frequency of the alternating current supplied to the induction coil. Transformers, generators, and electric machines are all operated in AC conditions. In addition to sufficient magnetic flux density, minimum energy loss is the most important consideration in AC applications.

Typical energy losses and their distribution in a 50 HP motor are shown in Fig. 1. One of the major energy losses directly related to soft magnetic materials is the iron loss, which increases with excitation frequency. For motors and transformer applications, a higher frequency is preferred because it can significantly improve power densities, as shown in Fig. 2. This is why reducing the iron loss at higher excitation frequencies is a major focus for most of the researchers on soft magnetic materials. The improvement of magnetic material properties is highly rewarding. For example, in a transformer, an increase of 1.5% in energy efficiency implies a direct saving of 240×10^9 kW·h [1], which is equivalent to $12 billion/yr for electricity price of $0.05/KW·h.

There are two main approaches to minimizing the AC iron losses according to the classic eddy current theory: (1) decreasing the part's thickness and (2) increasing the part's electrical resistivity. The traditional approach is to reduce the sheet thickness to 0.65–0.35 mm [5,6], and then coating the sheet with an electrically insulating layer. The resulting product is a stack of thin laminates insulated from each layer,

* Corresponding author at: Department of Material Science and Engineering, Iowa State University, Ames, IA 50011, United States.
E-mail address: gaoyuan@iastate.edu (G. Ouyang).

https://doi.org/10.1016/j.jmmm.2019.02.089
Received 3 October 2018; Received in revised form 17 January 2019; Accepted 26 February 2019
Available online 27 February 2019

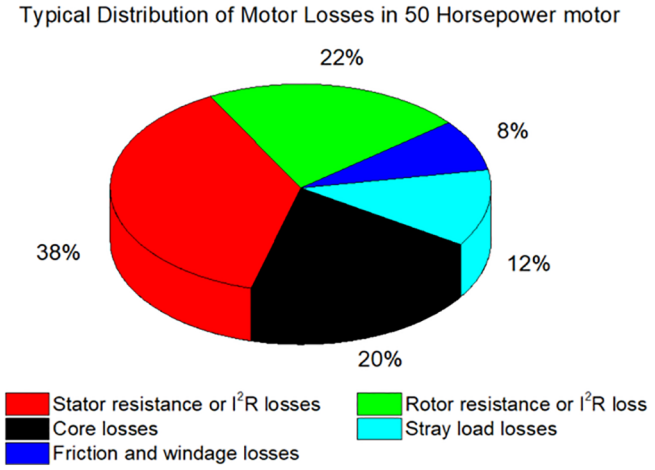

Fig. 1. Typical energy losses and their distribution in a 50 HP motor [2].

which satisfies both the low thickness and high resistivity requirements. Further reduction of the thickness to below 0.1 mm to meet the requirements of aircraft and aerospace applications [7] is possible [5,8–10] but not popular owing to the high processing cost and low stacking efficiency [10]. With the low-thickness approach reaching its practical limit, minimization of iron loss demands new soft magnetic materials with a high electrical resistivity. In addition to reducing the thickness and increasing the resistivity to minimize the classical eddy current loss, AC iron losses can also be lowered by tailoring the anisotropy and magnetization reversal processes, including domain wall engineering [11,12] and refinement of various structure parameters (e.g., impurities, defects, grain size [13], residual stress [14–16], and crystallographic texture [7,17]). Advanced and sophisticated metallurgical and manufacturing processes are usually required to maintain a low AC iron loss [5,18].

Besides high electrical resistivity, a high saturation magnetic flux density is also important. At a fixed frequency, a high magnetic flux density implies a high power density and high torque for motor application. With the increasing demand for higher performance, history has witnessed the invention of a variety of soft magnetic materials from mild steel around 1880 to silicon steel in 1900 [19], permalloys in 1915–1923 [20], ferrites in the 1940s [21], amorphous alloys in 1967 [22], high silicon steel in the 1970s [23], and nanocrystalline alloys in 1988 [24]. Soft magnetic materials are categorized into different subgroups based on their chemistry and composition. Typical soft magnetic materials that are available in the market [6] are pure iron and low-carbon steel, iron-silicon alloys (Fe and up to 6.5 wt% Si), iron-based sintered powders or the so-called powder core (Fe with minor alloying of P and/or Si), permalloy (Fe-Ni) or molypermalloy (Fe-Ni-Mo), permendur or hiperco (Fe-Co-V), MnZn or NiZn ferrites, sendust (Fe-Si-Al), Fe-based amorphous alloys (Fe-B-Si), Co-based amorphous alloys (Co-Fe-B-Si), and nanocrystalline alloys (HITPERM, NANOPERM, FINEMET). A collection of commercially available soft magnetic materials in the form of a toroid is shown in Fig. 3.

Each type of soft magnetic material has its distinct feature; for example, permalloy is known for its near-zero anisotropy and magnetostriction, and high permeability; however, it has either a low saturation magnetization, or a low electrical resistivity depending on the composition. Although permendur shows the largest room-temperature saturation magnetization [25], its eddy current loss is high due to its low electrical resistivity. Soft ferrites have excellent electrical resistivity, but also have a low saturation magnetization owing to its ferrimagnetic nature. Silicon steel offers high saturation magnetization and low cost, but its eddy current loss is yet to be improved. The amorphous and nanocrystalline alloys are unique owing to their exceptionally low coercivity and eddy current losses; however, they are extremely brittle and lacks high saturation magnetization [26].

Significant developments have taken place in these materials since their invention. New compositions and new devices along with advanced processing techniques were developed to improve the performance of ferrites [27,28]. Metallurgical advances with focus on optimizing texture, defects, impurities, grain size, and residual stress have been achieved in conventional silicon steel [7,29]. Key understanding of processing the steel with high silicon content and thinner gauge has been established [30]. And for the amorphous and nanocrystalline alloys, researches on improving saturation magnetization, thermal stability, and anisotropies [31–33] as well as new fabrication methods to integrate the brittle materials into devices are also making steady progresses [26]. Over the last decade, new nanocrystalline alloys with higher saturation magnetization and improved ductility have been developed. A notable example of high saturation nanocrystalline alloys is the Fe-Si-B-P-Cu alloys, trade name “NANOMET”, developed by Makino [200]. NANOMET shows a saturation magnetic flux density (Bs) as high as 1.9 T [200], and was recently demonstrated to be able to be made into 120mm-wide tapes [201]. While the Fe-Si based nanocrystalline materials made significant improvement in magnetization, the newly designed Co based [202] and FeNi based [203] nanocrystalline alloys made notable improvement in ductility. The ribbons pieces from these alloys showed improved fracture toughness by surviving simple bending tests during which the ribbons were bent into U shape without fracture [202,203]. These newly developed nanocrystalline alloys show great potential and are on the verge of widespread commercialization.

Among all the soft magnetic materials, silicon steel is still by far the most commonly used material with an annual worldwide production of ten million tons and a market share of 80% [30]. Silicon steel (3.2 wt% Si) is currently the most popular choice for motors and transformers because it offers balanced electrical and magnetic properties, and perhaps more importantly, low cost. It is composed of silicon and iron, two of the earth’s most abundant elements. In addition, the conventional 3.2 wt% silicon steel has excellent ductility, allowing the slabs coming out from the continuous casting line to be directly hot-rolled into hot-bands with 3 to 5 mm thickness, then cold-rolled into thin laminates of less than 1 mm thickness. Recently, with the market demand of further reduction in energy loss, a new generation of materials such as high silicon steel, amorphous alloys, and nanocrystalline materials have been intensively investigated. Unfortunately, none of these materials possesses all of the desired physical properties and all of them incur high processing costs. Figs. 4 and 5 compares the saturation magnetization, electrical resistivity, and iron loss of these materials at 1 T and 400 Hz, respectively. These figures show that 6.5 wt% silicon steel offers a good balance of high saturation magnetization (1.8 T) and high electrical resistivity (82 μΩ-cm), and low iron loss. In addition, high silicon steel displays near-zero magnetostriction [34], which is necessary for reducing the operating noise of transformers.

Despite these favorable properties, the application of high silicon steel remains mostly at the lab scale [41]. The main hindrance to its wide application is its high processing cost resulting from its brittleness. The material cannot be mass-produced using the economic cold roll process, which is widely used for low silicon steel. A majority of research conducted in the field of high silicon steel focuses on resolving the brittleness problem while maintaining and enhancing its magnetic properties. This paper reviews the history, structure, properties, processing, and applications of high silicon steel.

2. History of high silicon steel

The beginning of silicon steel started at the turn of the 20th century when the developing world was expanding, and with it, the demand for the generation and transportation of electrical energy was increasing. An English scientist named Robert A. Hadfield began investigating methods to improve the soft magnetic material of choice at that time: pure iron. He began by introducing various elements, creating several

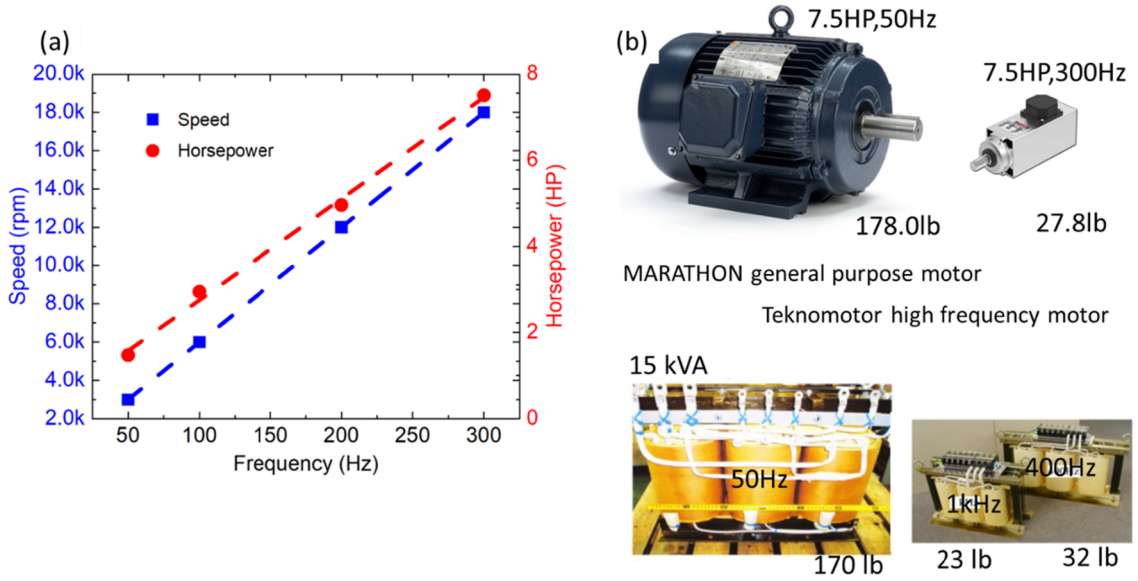

Fig. 2. (a) Plot of power density vs frequency for a motor. (b) Comparison of power densities of a low-frequency motor/transformer and a high-frequency motor/transformer. The size is significantly reduced by the use of high frequencies in both cases [3,4].

iron alloys, and observing the effects of alloying elements on its magnetic and electrical properties. He began looking at carbon, aluminum, nickel, and silicon. The majority of these additions sacrificed much of the material's magnetic saturation without imparting enough beneficial effects. However, silicon, while still decreasing the overall magnetic strength, was able to dramatically improve the magnetic permeability, and electrical resistivity, while decreasing the coercivity [19]. His findings were further investigated by Guimlich in 1912 and Campbell in 1920, who confirmed that the addition of up to 6.5 wt% silicon yielded the best electrical and magnetic properties [42,43]. The only drawback to this addition was that above 3.2 wt% silicon, the material becomes brittle and difficult to work with using the traditional manufacturing methods. Therefore, for the time, 3.2 wt% silicon became the gold standard of soft magnetic materials.

Around 1930, Norman P. Goss was looking into ways to further improve the 3.2 wt% silicon steel, which were then used in the American electrical grid. The original method for processing the material left it with isotropic properties with a random orientation of grains. The crystal structure of silicon steels has an easy magnetic direction of ⟨1 0 0⟩, a medium direction of ⟨1 1 0⟩, and the worst direction of ⟨1 1 1⟩. Goss developed a method of orienting the silicon steel grains with a ⟨1 0 0⟩ texture, such that the subsequent processing would selectively encourage their growth and result in grain-oriented silicon steel. The grain-oriented silicon steel exhibited increased permeability and a significant reduction in iron loss in the rolling direction, perfect for high-voltage power transformers [44].

As the demand for more powerful and efficient means of producing 3.2 wt% silicon steel increased over the next 40 years, much of that time was spent refining various processing techniques in an attempt to extract as much performance as possible. Beginning around the

Fig. 3. Photo showing a collection of commercially available soft magnetic materials in toroid form. Three differently sized samples are wound with primary (outer, yellow color wire) and secondary (inner, red color wire) windings for magnetic measurement. Note that there are several tiny sharp fragments beneath the nanocrystalline core. The tape shattered into fragments during uncoiling owing to the brittle nature of the nanocrystalline sample. (For interpretation of the references to color in this figure legend, the reader is referred to the web version of this article.)

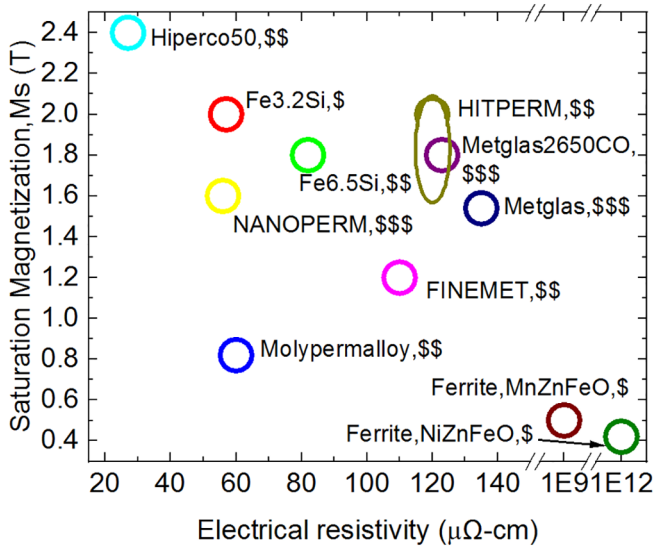

Fig. 4. Comparison of electrical resistivity and saturation magnetization of a few key soft magnetic materials [9,31,35–40].

1970 s, the demand for a soft magnetic material with exceptional electrical resistivity for high-frequency audio equipment brought 6.5 wt% silicon steel back into the limelight. Its inherently higher electrical resistivity and near-zero magnetostriction made it a perfect material for applications at high frequencies as it could minimize losses from both eddy current loss and shape changes [23]. This sparked a renewed effort to find alternative ways to process the brittle material, and many methods were tested over the next few years including melt spinning, chemical vapor deposition (CVD), twin rolling, and powder metallurgy [45–48]. Melt spinning showed great promise in producing a low-cost 6.5 wt% silicon steel [49–51]. As demonstrated by Liang et al. [51], 30-mm-wide continuous tapes could be successfully produced by melt spinning, and their excellent ductility ensured that the tapes could be coiled into spools. However, the industry did not switch over immediately to 6.5 wt% silicon steel due to the increased cost, and it is only with the recent demand for even more efficient electric motors and high-voltage transformers that the high silicon steel is finally on the verge of being accepted as a commercially viable soft magnetic material [51].

3. Structure of high silicon steel

3.1. Effect of silicon in steel

Silicon addition in steel has several profound effects. Due to the smaller atomic radius of Si (1.11 Å) than that of Fe (1.26 Å), the lattice parameter of Fe-Si decreases linearly from 0 to 18 wt% of silicon content [34,52]. A change in slope occurs at around 5 wt% of silicon that corresponds to the ordering, as will be discussed in detail below. The density of Fe-Si follows the same trend as that of the lattice parameter, and Fe-6.5 wt%Si has a density of 7.48 g/cc [34].

Silicon addition rapidly increases the electrical resistivity of iron [52]. The electrical resistivity of 6.5 wt% Si steel is 82 μΩ-cm, while that of pure iron is 10 μΩ-cm [7,34]. Arato et al. [53] found that Si addition increases the electrical resistivity linearly with a coefficient of 11.62 μΩ-cm per wt% in the range of 0.15–2.2 wt% silicon steel. A similar coefficient of 12.785 μΩ-cm per wt% was measured by Hou [54] with the silicon content ranging from 0.21 to 2.0 wt%. In practice, the silicon content was back-calculated by measuring the electrical resistivity by NKK corporation in the production line due to the near-linear relationship between resistivity and silicon content over the range of 3–8 wt% [35]. The increase in electrical resistivity results in lower eddy current loss [8,34,55] and higher efficiency. Ruder found that steel with 6.5 wt% Si has the lowest total loss at 1 T magnetic induction and 60 Hz induction frequency [56].

The magnetocrystalline anisotropy also decreases with silicon addition [7], thus resulting in higher relative permeability for high silicon steel [1]. The relative permeability was shown to increase slowly below 3 wt% silicon, then increase rapidly reaching a maximum of 29,000 at around 6.5 wt% silicon content before it drops [34]. The magnetostriction decreases rapidly along the ⟨1 0 0⟩ axes with increasing silicon content, while it increases slowly along the ⟨1 1 1⟩ axes, resulting in nearly zero combined magnetostriction for 6.5 wt% silicon steel [34,35,47]. The minimum magnetostriction can effectively reduce the transformer noise [47]. The saturation magnetization, however, decreases with increasing silicon content, reaching ~1.8 T at 6.5 wt% silicon [7,34]. In addition, the materials become more brittle with increasing silicon content due to the formation of ordered phases.

3.2. Ordering in high silicon steel

Fe-Si electrical steels have a substitutional A2 body-centered cubic (bcc) structure at low silicon concentrations. When the silicon concentration is increased to about 5.3 wt%, B2 ordering starts to occur

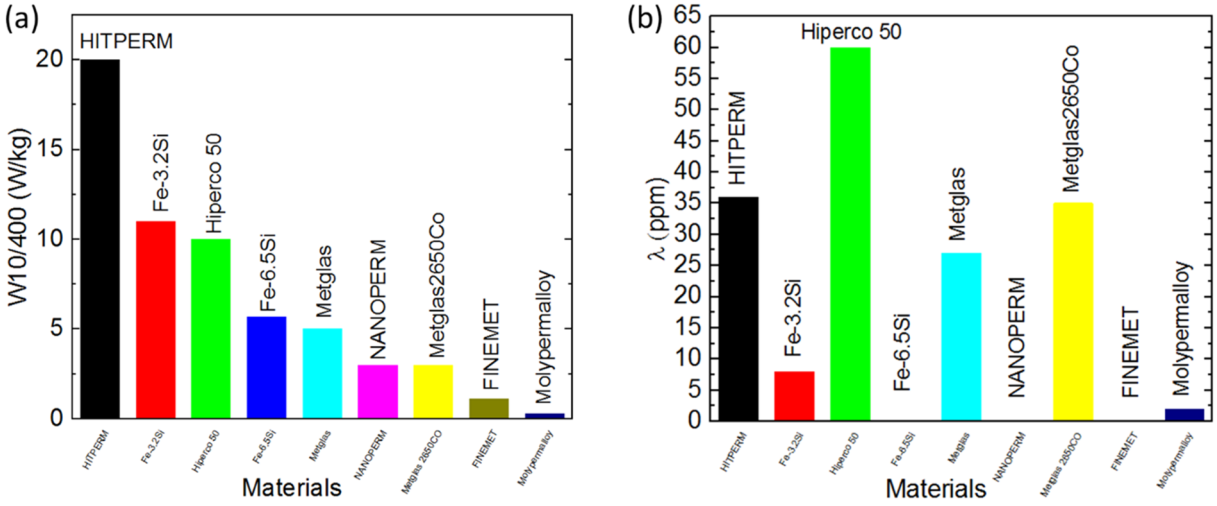

Fig. 5. Comparison of iron loss W10/400 (a) and magnetostriction (b) of a few key soft magnetic materials [9,31,35–40]. Note that the magnetostriction of 6.5 wt% Si steel is too small (0.01 ppm) to be shown.

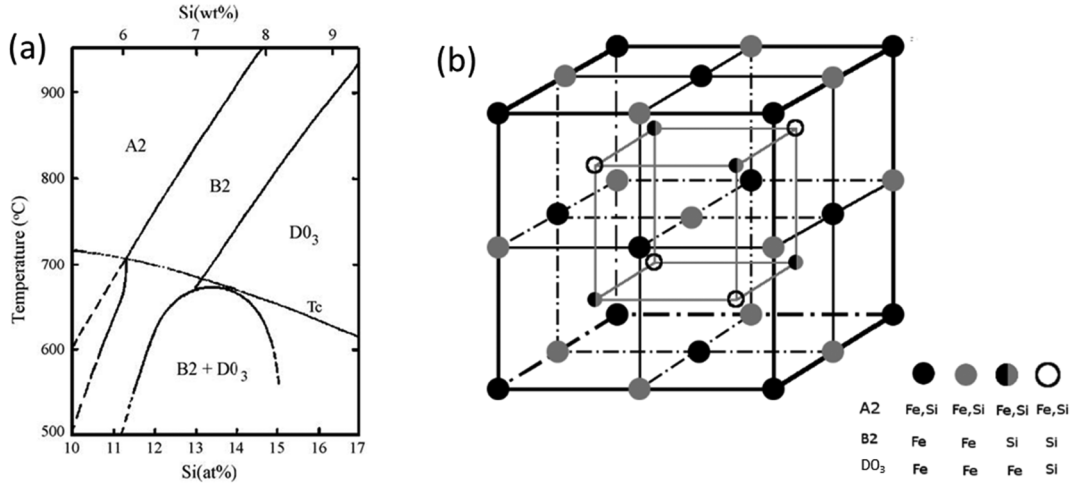

Fig. 6. (a) Fe-Si phase diagram of high silicon steel [57,58]. (b) Superlattice crystal lattice of high silicon steel. For disordered A2 phase, Fe and Si can sit in any of the plotted sites. For B2, Fe prefers the sites denoted by solid black dots and gray dots, while Si prefers the sites denoted by gradient dots and open dots. For $D0_3$, Si prefers the sites denoted by open dots, while Fe prefers all the other sites.

below 500 °C according to the phase diagram shown in Fig. 6a [57,58]. $D0_3$ ordering starts to appear when the silicon content is increased beyond 6 wt%. The terms A2, B2, and $D0_3$ are Strukturbericht symbols that specify the structure of a crystal, and represents monatomic bcc α-Fe, CsCl-type AB compounds, and $AlFe_3$-type A_mB_n compounds, respectively. The ordering of Fe-Si can be best described using the superlattice structure consisting of four interpenetrating face-centered cube (fcc) cells having a lattice parameter twice that of a single bcc cell [58], as depicted in Fig. 6b.

The superlattice structure can also be viewed as consisting of 8 bcc lattices stacked as a cube. A2 is in the disordered state, with random distribution of iron and silicon atoms in the superlattice. The unlike-atom pairing of the nearest-neighboring atoms results in B2 ordering, where the sublattice sites are preferably occupied by silicon atoms. Further ordering between the next-nearest-neighboring atoms results in $D0_3$ ordering, where only half of the sublattice sites with the longest separation are preferably occupied by silicon atoms. It should be noted that the full B2 structure requires all sublattice sites (bcc sites) to be occupied, corresponding to the stoichiometric compound FeSi. Fe-6.5 wt%Si has insufficient silicon to form the stoichiometric compound. The B2 phase in Fe-6.5 wt%Si adopts the structure, wherein silicon atoms occupy some of the sublattice sites (bcc sites) and iron atoms fill rest of the sites. Similarly, the full $D0_3$ configuration requires 4 silicon atoms and 12 iron atoms, which correspond to the stoichiometric compound Fe_3Si. The $D0_3$ structure in Fe-6.5 wt%Si represents the structure in which silicon and iron tend to occupy the sites in the same manner as they do in Fe_3Si $D0_3$.

Due to the ordering, additional dots or lines appear on the electron or X-ray diffraction patterns [59]. These superlattice dots or lines are used for material characterization to determine the presence of B2 and $D0_3$ phases. $D0_3$ generates a unique superlattice peak corresponding to the {1 1 1} planes, while B2 shares the {2 0 0} superlattice peak with the $D0_3$ {1 0 0} planes. The ordering interacts with dislocations resulting in a strengthening effect [60], which adversely affects the mechanical properties. Superdislocation slip deformation mechanism as proposed for B2 and $D0_3$ lattices [61] also deteriorates the mechanical properties. B2 and $D0_3$ ordering leads to improved magnetic properties, where B2 growth is responsible for higher specific magnetization, and $D0_3$ growth is responsible for low magnetostriction, high maximum permeability, and low coercive force [62].

3.3. Suppression of ordering in silicon steel

To suppress the deleterious ordering, a variety of fast quenching routes has been explored. Raviprasad et al. [63] examined the ordering of rapidly solidified Fe-6.5 wt%Si by three processing routes: planar flow casting (PFC), melt spinning (MS), and twin rolling (TR). TEM analysis revealed that B2 ordering can be found in the single-roll-processed (PFC and MS) samples, while the additional $D0_3$ ordering can only be found in the twin-rolled samples. In addition, the B2 domains were also found to increase from 20 to 30 nm in the PFC and MS samples to 60 nm in the TR sample. This study suggested a strong dependence of ordering on cooling rate. The typical tangential wheel speeds used by these techniques were 8–60, 42, and 32 m/s, respectively. But, the actual cooling rates associated with each wheel speed for each method were not investigated.

The cooling process using three quench media was studied by Zhang et al. [64]. The cooling rates of oil, water, and salt water (10% NaCl) were found to be 74, 304, and 375 °C/s, respectively, for the samples with dimensions of 2 mm × 5 mm × 35 mm. The faster cooling rates resulted in a reduction of the ordered region with the domain sizes changing from 1 to 3 μm to 20–200 nm and 5–50 nm, respectively. However, a higher cooling rate was found to create larger residual tensile stress, which to certain degree, diminishes the ductility gained by lowering the degree of ordering.

Fu et al. [61] studied the effect of cooling rate on Fe-6.5 wt%Si-0.05 wt%B alloy with columnar grains formed by directional solidification. Rapid oil quenching reduces the growth of needle-shaped boron-rich precipitates that are harmful to the bending properties. The size of the ordered phase reduces from 3 to 5 μm to 20–50 nm, suggesting a reduction in the degree of ordering from furnace cooling to oil quenching.

It appears that rapid cooling can suppress the formation of $D0_3$ and reduce the size of B2, but cannot completely suppress the B2 ordering [65]. A summary of the relationship between known cooling rate and the resulting ordering is shown in Fig. 7.

In addition to quenching, deformation was also found to have effect in decreasing the ordering and reducing brittleness. Fu et al. [68] found that the superlattice B2 and $D0_3$ peaks were missing in the TEM diffractions patterns after compressing the sample at room temperature, and the compression deformation allowed the sample to be warm and cold rolled to a 0.2-mm-thick sheet with no obvious edge cracks.

4. Properties of high silicon steel

4.1. Magnetic properties

High silicon steel can be used in both direct current (DC) and

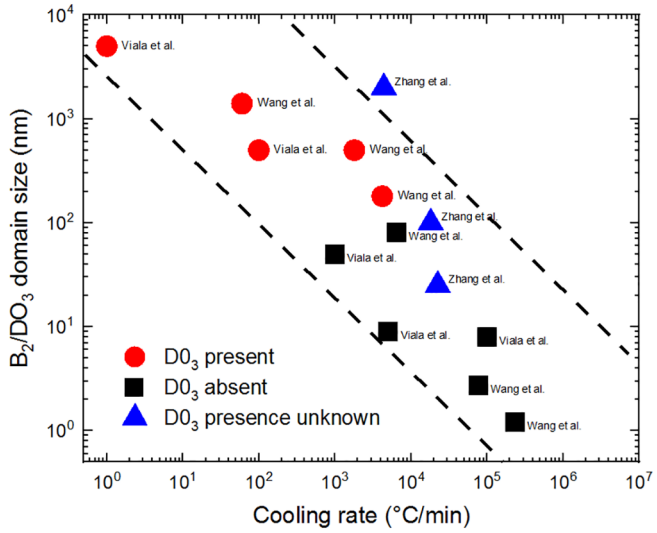

Fig. 7. B2/DO_3 ordering as a function of cooling rate. Red circles indicate the presence of DO_3 phase, and black squares indicate the absence of DO_3 phase. The presence of DO_3 is unknown in the case of blue triangles [64,66,67]. (For interpretation of the references to color in this figure legend, the reader is referred to the web version of this article.)

alternating current (AC) applications. Its DC and AC magnetic properties are equally important. Permeability, magnetic flux density, and coercive field are the key properties for DC applications, while iron loss including hysteresis loss, eddy current loss, and anomalous loss are the most important properties for AC applications.

4.1.1. DC magnetic properties

The permeability of hot-rolled and annealed silicon steels with the silicon content ranging from 0.21 to 2.0 wt% was studied by Hou [54]. Grain size was found to be the predominant factor for permeability at a low induction (1 T) for both DC and AC 50 Hz conditions. Under a high induction, i.e., 1.5 T, the ⟨2 0 0⟩ out-of-plane texture component was found to have greater influence. The magnetic flux density was found to increase with increasing ⟨2 0 0⟩ texture component, while the effect of grain size was insignificant. The coercivity is inversely proportional to grain size for polycrystalline magnetic materials with grain sizes above 150 nm following the 1/D law [69,70]. With decreasing coercivity, the permeability increases, as they are inversely related [70]. Chemistry also plays a role in coercivity. Arai and Tsuya [49] showed that, compared to other compositions, 6.5 wt% silicon steel displayed the lowest coercive field. Further, iron loss occurs in DC application as hysteresis loss as well, but it is generally not a major concern.

4.1.2. AC magnetic properties (iron loss)

Iron loss is one of the most important properties of soft magnetic materials used in AC conditions. Iron loss is the energy loss (in watt/kilogram or watt/pound) per cycle at a specific frequency and flux density [1]. Iron loss is expressed as "Wa/b", where "a" is the magnetic flux density in Kilogauss (KG) or one-tenth of a Tesla (T), and "b" is the frequency in Hz. For example, W10/400 denotes the total iron loss at 10 KG or 1 T magnetic induction with 400 Hz frequency.

The iron loss for sinusoidal excitation can be approximated using empirical equation in the form of Steinmetz equation:

$$P_v = C_v f^{\alpha} B_m^{\beta} \tag{1}$$

where P_v is the power loss per volume; f is the frequency; B_m is the peak magnetic flux density; and C_v, α, and β are the three fitted so-called Steinmetz parameters. The very first formula derived by Steinmetz does not have the frequency term, and β was determined to be 1.6 for hysteresis losses and 2 for eddy current losses [71]. The three Steinmetz

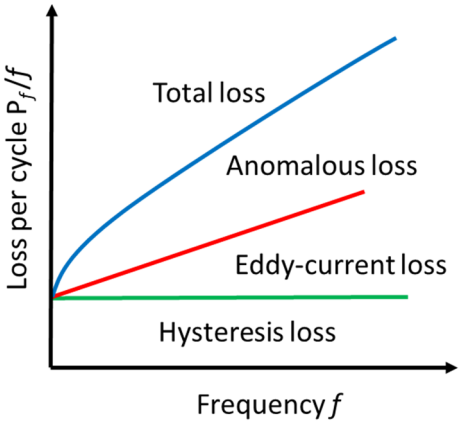

Fig. 8. Schematic of iron loss separation as a function of frequency [1,75].

parameters in Eq. (1) vary for different materials and testing frequencies, and are usually published by soft magnetic material manufacturers for their products. The Steinmetz equation can also be extended into the non-sinusoidal excitation with modification [72–74].

The iron loss can be better understood by the loss separation approach [75]. The iron loss consists of hysteresis loss, eddy current loss, and anomalous loss (sometimes called excess loss), with eddy current loss being the major contributor at frequencies higher than 400 Hz. The contribution of each component as a function of frequency is illustrated in Fig. 8 [1,75].

Hysteresis loss per cycle is the energy loss when the material is cycled once between a positive and negative applied field. It is the area enclosed by the B versus H loop. Hysteresis loss can be determined experimentally by the DC magnetic measurement of a single BH loop.

The eddy current loss is created by the electromotive force (emf) caused by the alternating magnetic flux. Its direction is always opposite to the magnetic field, thereby reducing the flux change according to Lenz's law. Its magnitude is proportional to the change in magnetic flux and the cross-section area of the material. The eddy current generates heat, causing power loss proportional to the square of the eddy current and the resistance. Eddy current loss (classical) can be calculated assuming complete flux penetration and constant permeability, and strongly depends on d, f, and B_0 [1].

$$P = \frac{10^{-9}\pi^2 d^2 B_0^2 f^2}{6\rho} \frac{erg}{\sec\ cm^3} \tag{2}$$

where d is the thickness in cm, B_0 is the surface flux density in Gauss, f is the frequency in Hz, and ρ is the resistivity in Ω-cm. The unit resulted for P is erg/sec cm^3. It converts to watt/cm^3 when multiplies by 10^{-7}.

Classical eddy current estimation through Maxwell's equations assumes that the material is completely homogenous and devoid of domains [76]. The existence of magnetic domain structures results in a more complex and non-uniform distribution of eddy currents [6]. The classical eddy current theory tends to underestimate the total iron loss. The excess eddy current loss component that cannot be explained through the classical model of uniform magnetization is called anomalous loss [6]. Since it is merely eddy current loss that is not calculable in detail, some researchers had suggested that the anomalous loss be renamed as excess eddy current loss [76]. A common practice in estimating the anomalous loss (Pa) is to subtract the hysteresis loss (Ph) measured under DC condition and the eddy current loss (Pe) calculated from the classical formula from the measured total iron losses [76]. A more complex evaluation of eddy current loss is presented by Pry and Bean [77] by considering the domain structure effect. The domain model eddy current loss is larger than the classic model power loss, and the ratio between these two values increases with an increase in 2L/d, where L is the domain size and d is the sheet thickness. When the domain size is constant, the classic model tends to underestimate more for

a thinner sheet [1].

The magnitude of eddy currents is not uniform along the entire specimen. The eddy currents are the strongest at the center, where all the current rings add, and weaken toward the surface [1]. As a result, the H and hence B inside the body can be much lowered than that on the surface, especially in a thick specimen. This causes shielding of the interior of the thick specimen from the applied field, which is called the skin effect. The field, H_x, and flux density amplitude, B_x, inside the specimen at a distant × below the surface can be calculated using the following equation, assuming that the permeability, μ, is constant everywhere in the specimen and under any field [1].

$$\frac{H_x}{H_0} = \frac{B_x}{B_0} = \left[\frac{\cosh\left(\frac{2x}{\delta}\right) + \cos\left(\frac{2x}{\delta}\right)}{\cosh\left(\frac{d}{\delta}\right) + \cos\left(\frac{d}{\delta}\right)} \right]^{\frac{1}{2}} \tag{3}$$

$$\delta = 5030\sqrt{\frac{\rho}{\mu f}}\ \text{cm} \tag{4}$$

here, the field is applied parallel to the surface of the sheet and vary sinusoidally with time as $H = H_0 cos 2\pi ft$, where d is the sheet thickness in cm, δ is the "skin depth," ρ is the resistivity in Ω-cm, and f is the frequency in Hz. Skin depth is the depth under the surface where H_x or B_x drops to 1/e (~37%).

4.2. Iron loss management

Iron loss can be affected by silicon content, grain size, impurities, and texture [78]. Larger grains result in smaller coercivity and higher permeability, both of which lead to lower hysteresis. However, on the contrary, larger grains tend to result in larger eddy current loss and anomalous loss [79,80]. Shimanaka et al. [8] found that the desired grain size for the lowest W15/50 lies between 100 and 150 μm for 1.85–3.2 wt% Si, with the high silicon content requiring larger grain sizes. Hou [54] found that hysteresis loss and eddy current loss decrease with increasing silicon content from 0.21 to 2.0 wt%. The reduction in hysteresis loss was mainly due to texture and grain size, and the reduction in eddy current loss was primarily due to the increase in resistivity. For the frequency range of 1–1000 Hz, Campos et al. [80] proposed a model to roughly estimate the optimum grain size, which states that the optimum size is dependent on resistivity, frequency, and sheet thickness. The optimum grain size of a 0.51-mm-thick electric steel was estimated by Campos et al. to be in the range of 163–110 μm for the frequency range of 30–100 Hz.

Impurities, especially fine particles, results in an increase in hysteresis loss due to the pinning of domain wall motion and grain growth [8]. Carbon and nitrogen are usually reduced to 40 ppm and 20 ppm by moist hydrogen annealing and Al addition, respectively [8]. Reduction in sulfur content from 65 ppm to 4 ppm can also result in a lower hysteresis loss, as shown by Oda et al. [81]. Aluminum addition reduces free nitrogen by forming AlN, which also improves the texture [8]. However, the presence of aluminum oxide particles increases the rate of wear of the punch-out dies [1]. Other alloy additions such as Sb, Cr, and B have been explored. Antimony addition was shown to result in both lower loss and higher permeability [82]. Komatsubara et al. [83] studied 4 wt% Cr addition in 4.5 wt% silicon steel in Kawasaki Steel Corporation. The alloyed steel exhibited good workability owing to its low Vickers hardness of 240 HV and offered lower iron loss at high frequencies over 5 kHz. However, its iron loss at low frequencies including 400 Hz and 1 KHz was worse than that of 3.2 wt% silicon steel and 6.5 wt% silicon steel. Kim et al. [84] showed that boron addition up to 530 ppm into 6.5 wt% silicon steel improved the workability due to grain refinement resulting from boron grain boundary segregation.

Texture also affects the iron loss, with lower loss present in the (1 0 0) plane followed by (1 1 0) and (1 1 1) planes [8], corresponding to the easy magnetization axis of ⟨1 0 0⟩ and hard magnetization axis of ⟨1 1 1⟩ in bcc iron. Texture can be achieved in electric steel through the following routes: (1) utilizing the γ to α transition (fcc to bcc structure) during cooling [8]; (2) recrystallization and annealing after heavy cold-rolling [1,8,85]; (3) rapid solidification [86–88]; (4) directional solidification/recrystallization [89–91]; (5) alloying addition [82,8]; and (6) magnetic annealing [92–95]. The desired texture for the stationary transformer and for the motor are different. For transformers, the field is along the long edges of the laminations. Easy ⟨1 0 0⟩ direction in the direction of magnetization is preferred, and the desired texture is {*hkl*} ⟨1 0 0⟩. In practice, grain-oriented steels were so prepared that they have the {1 1 0} ⟨0 0 1⟩ GOSS texture. For motor, the field is in the plane of the sheet, while the angle in the plane rotates. {1 0 0} < uvw > is satisfactory as it keeps the hard ⟨1 1 1⟩ axis out of the plane, and ⟨1 0 0⟩ out-of-plane fiber texture is more favorable, as it would be isotropic in the sheet plane [1]. Moreover, although a cube texture {1 0 0} ⟨1 0 0⟩ has been achieved, it has not been produced in large quantity [1].

The anomalous loss is also affected by domain sizes and the number of domain walls [76]. Decreasing the domain size [12] and increasing the number of domain walls reduce the anomalous loss [76]. A number of domain-refining techniques have been proposed to reduce the anomalous loss [12,76]. Typical methods include grain size refinement, application of stress through coating [96], laser irradiation [97], laser scribing [45], and introduction of local strain [98].

4.3. Lamination and near-net shape processing

The effect of thickness on iron loss can be large. Oda et al. showed a 25%–30% iron loss reduction for W10/400 when the thickness of the electric steel was reduced from 0.35 mm to 0.20 mm [99]. Kan et al. [55] also showed similar results for W12.5/50 for ribbons with 100 μm thickness. Due to the skin depth problem, silicon steel is mostly used in the laminated form to reduce energy loss. Thin paper was historically used by George Westinghouse to laminate wrought iron sheets to make transformers in 1885 [100]. Nowadays, a coating is applied to each thin silicon steel laminate for electrical insulation. A few coating strategies are available: organic varnish can be used, but it cannot withstand the stress-relief annealing; a slightly oxidizing annealing atmosphere can be used to form an iron oxide film that tightly adheres on the surface; and MgO powder coating is often used before high-temperature annealing. MgO powder combines with SiO_2 to form a glassy magnesium silicate, and puts the steel in tension after cooling to room temperature due to a smaller CTE, which may also result in lower core losses due to the favoring of 180° domain walls [1].

The insulating coating, not being a ferromagnetic material, lowers the effective volume of the electric steel. In addition, the coating and laminating process adds additional labor to the production. Moreover, the magnetic properties including AC loss and magnetizing force H15/50 (H15/50 is the magnetic field required to reach a magnetic induction of 1.5 T at 50 Hz) of silicon steel can be severely affected by the stamping method used to prepare the laminates. According to Kurosaki et al. [101], the strains produced during shearing and laser cutting resulted in higher W15/50 and H15/50 compared to the strain-free laminates obtained by wire electrical discharge machining (WEDM). Subsequent annealing at 750 °C for 2 h to relieve stress can be used to eliminate the difference. The authors also reported that the interlocking and welding used to clamp the laminates led to higher eddy current losses due to short circuits.

Near-net shape processing of insulated electric steel may offer a solution to this dilemma. Composites of insulated soft magnetic materials are often called soft magnetic composites (SMCs). Shokrollachi et al. recently reviewed SMCs [102]. The insulating coating can be organic or inorganic, where the organic coatings typically are epoxy, acrylic, polyester, epoxy-polyester hybrid, and polyurethane, and the inorganic coating can be an oxide (such as Fe_2O_3), a phosphate (such as zinc phosphate, iron phosphate, and manganese phosphate), or a

sulfate. SMCs are attractive owing to their low eddy current loss, which is made possible by the high resistivity offered by the inter-particle insulation. Its ability to undergo near-net shape processing via the powder metallurgy compaction route is also an advantage. However, the coating and the air–gap dilute the material's saturation magnetization and permeability. In addition, higher hysteresis losses are often observed due to the strain produced during the compaction.

Recently, by mixing with a 35 vol% wax-based binder, near-net shaping of an atomized 12.7 μm Fe-6.5 wt%Si powder compact was made possible via metal injection molding by Miura and Kang [103]. Followed by solvent debinding, thermal debinding, and 1350 °C sintering, a nearly 100% dense body was produced. However, the DC magnetic properties of the sintered compact were not as good as that of the wrought Fe-6.5 wt% alloy. And the iron loss of ~ 400 W/kg at 10 kHz is high. Such high iron loss was probably resulted from the lack of lamination of the sintered body. In another study, a nearly fully dense Fe-6.5 wt%Si/SiO_2 core–shell composite was synthesized [104]. The process involves ball milling of water-atomized Fe-6.5 wt%Si alloy powders and SiO_2 powders followed by spark plasma sintering at 1150 °C. The composite has an excellent electrical resistivity of 1400 μΩ-cm. However, both the coated and un-coated Fe-6.5 wt%Si compacts suffered from poor DC and AC magnetic properties. A new in situ chemical deposition process using 3-aminporophyltriethoxysilane (APTES), tetraethyl orthosilicate (TEOS), anhydrous ethanol, and ammonia was used to replace the ball milling process, yielding a remarkably high electrical resistivity of 4800 μΩ-cm [105]. W10/400 of 10.6 W/kg was achieved on a 6.35 mm composites compact, which was similar to that of a commercial thin 6.5 wt% silicon steel sheet [105]. However, the newly produced thin composites had lower saturation magnetization and permeability caused by the addition of SiO_2.

It should be noted that all the conventional bulk magnets use either sheets, or near-spherical powders as building blocks. A new strategy was proposed by Cui et al. using the coated flakes, which offers new method to minimize the saturation magnetization loss while maintaining high electrical resistivity [106]. The flakes can be mass-produced by melt spinning, coated with a nonconductive coating, and then consolidated into bulk magnets with a "brick wall" structure, as shown in Fig. 9. This strategy uses ductile flakes instead of sheets or powders as building blocks for the bulk magnet. The use of flakes is different from using sheets in that near-net shape processing can be achieved, and differs from using powder of the same thickness in that the demagnetization factor and eddy current can be minimized. A limitation of the flakes approach is the relatively low packing density, which can lead to low density and low magnetization. It, however, offers endless possibilities to optimize the flake size, spacing, and the coating thickness for specific frequencies and induction levels.

4.4. Mechanical properties

Tensile tests performed by Seifert et al. [107] on double-roller-quenched and annealed Fe-6.5 wt%Si steel suggested that the appearance of $D0_3$ superlattice structure is responsible for the loss of ductility. They also showed that the ductile as-quenched samples could be converted into brittle materials by air cooling or annealing, and brittle ribbons can be converted back into ductile ribbons by annealing above the B2-$D0_3$ temperature followed by quenching; this further supports the argument that $D0_3$ ordering renders the Fe-6.5 wt%Si steel brittle. Higher bending numbers were observed on thinner samples, and the increased ductility of thinner ribbon was claimed to be caused by the greater mobility of dislocations in the surface region.

The stress–strain curves and XRD patterns of the melt-spun Fe-6.5 wt%Si ribbon in the as-spun state and annealed state are shown in Fig. 10a and b, respectively. After annealing at 1100 °C, the annealed sample was slowly cooled at a rate 10 °C/min. The annealed sample exhibited worse mechanical properties than the rapidly quenched sample did, as demonstrated by lower strength and less elongation at break. XRD analysis revealed the formation of B2 and $D0_3$ in the annealed sample, which is responsible for the loss of ductility. However, as compared to the ductile as-spun state, annealing improves the magnetic properties including relative permeability and coercive force, as shown in Fig. 10c. It also reduces the iron loss at 400 Hz and 1000 Hz, as shown in Fig. 10d. Production in the ductile state followed by a final annealing prior to application is key for the production of high silicon steel with the desired magnetic properties.

The hardness increases monotonically with increasing silicon content according to Hou [54], who studied steel with a maximum silicon content of 2.0 wt%. Shin et al. [57] studied the hardness of silicon content up to 13 at% by micro-indentation and nanoindentation tests. Vickers hardness was found to vary linearly with silicon content. For high silicon steel, the equation HV = -112 + 41.1 at% Si was established, and for low (less than 6 at%) silicon steel, the equation HV = 59.9 + 24.3 $(at\%)^{2/3}$ was found valid. The $(at\%)^{2/3}$ and at% correspond well with substitutional solution hardening and short-range ordering hardening, respectively [108]. Nanoindentation showed two peak values, 5.55 GPa and 6.25 GPa, for the 100 indents made on the sample annealed at 650 °C for 2 h and then furnace cooled, which had both A2 and B2; this was the only result that suggested that A2 and B2 phases might have different hardnesses. Haiji et al. [35] showed that the workability can be further improved by suppressing grain boundary oxidation. The presence of oxygen during annealing was shown to reside in the grain boundaries, facilitating grain boundary rupture, which can result in poor workability.

To increase the ductility of high silicon steel, various alloying additions have been explored. Al [109], Ga, Cr, Ni, and Nb were found to

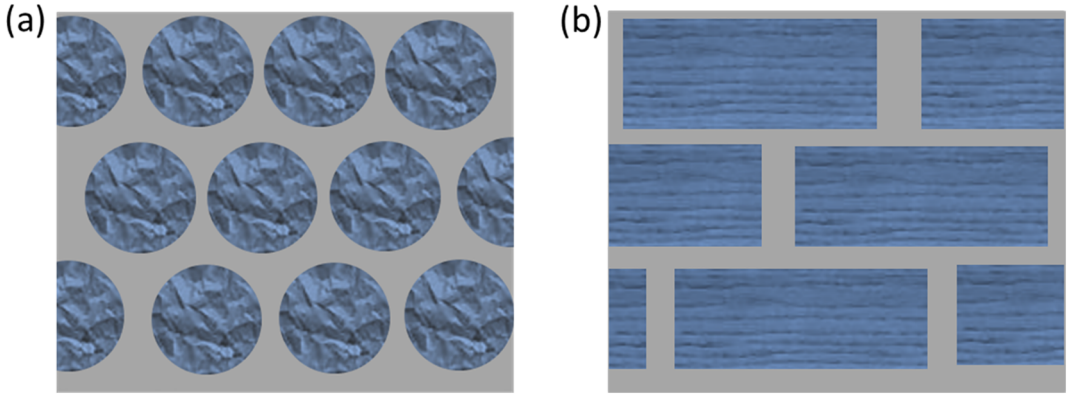

Fig. 9. Schematic showing a magnetic material consisting of (a) conventional spherical powders and (b) high-aspect ratio flakes. The powders and flakes are in blue and the coating is in gray. For comparison, the thickness of the flakes is equal to the diameter of the powder. (For interpretation of the references to color in this figure legend, the reader is referred to the web version of this article.)

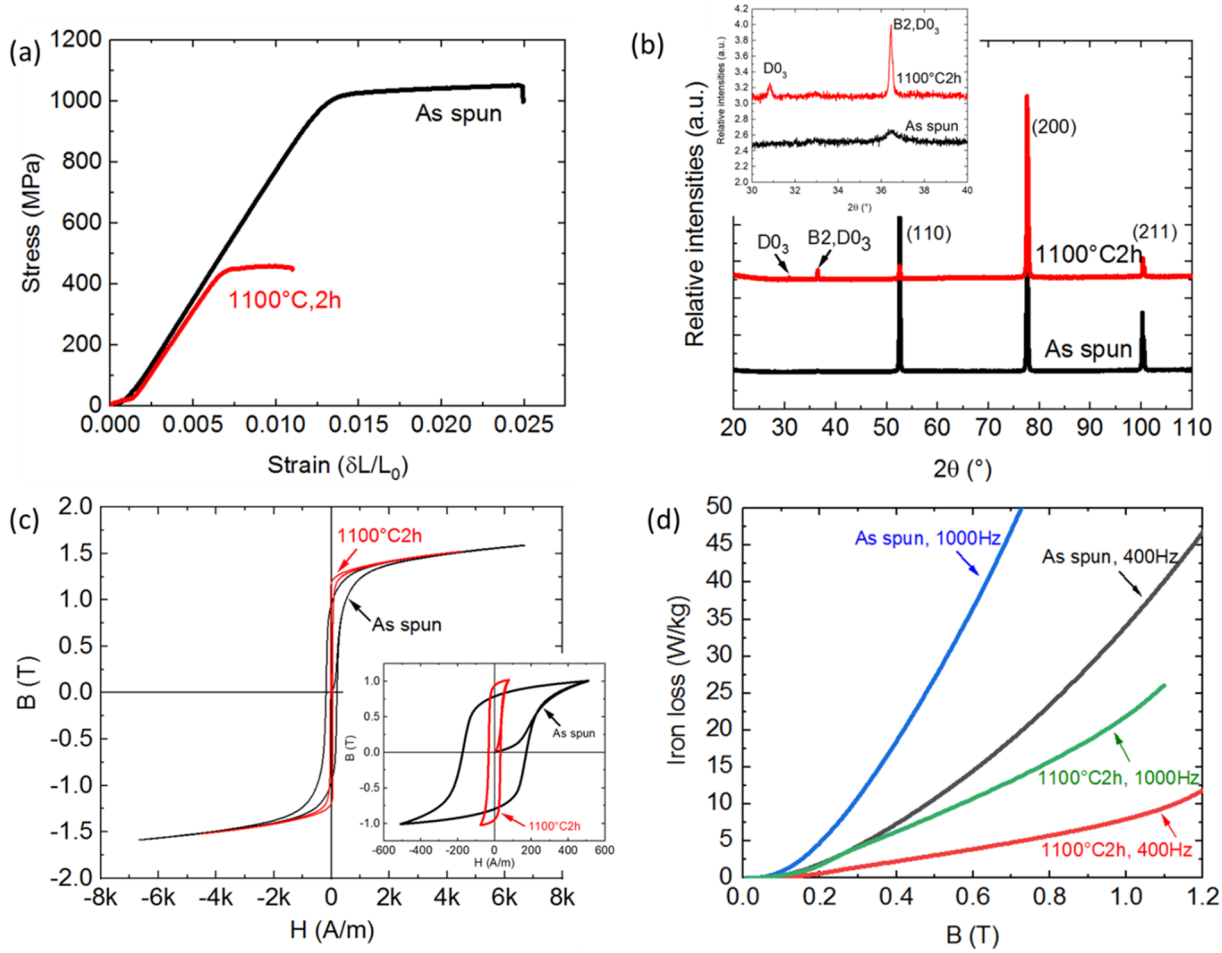

Fig. 10. (a) Stress–strain curves of Fe-6.5 wt%Si steel strips tested in as-spun state and annealed state followed by slow cooling at 10 °C/min rate. The strain was measured by grip-to-grip separation. (b) XRD patterns of Fe-6.5 wt%Si steel in as-spun state and annealed state followed by slow cooling at 10 °C/min. The insert shows the superlattice peaks. (c) BH loops for Fe-6.5 wt%Si tape-wound core in as-spun state and annealed state tested up to 8000 A/m using KJS Associates/ Magnetic Instrumentation Model SMT-700 Soft Magnetic Tester. The inset shows the BH loops with 1 T peak magnetic flux densities. (d) Total iron losses of the Fe-6.5 wt%Si tape-wound cores as a function of flux density at different frequencies in the as-spun state and annealed state.

increase the plasticity of high silicon steel [110]. However, the amount of alloying additions has to be restricted to a limited quantity, i.e., 2%, or in the case of Nb at 0.5%, due to the adverse effect on magnetic properties [110]. Mn addition was also explored and showed a more prominent effect than Ni in terms of ductility [111]. Kim et al. [84] reported significant improvement in the workability of high silicon steel with the addition of up to 530 ppm boron, which allowed cold working of thin high silicon steel when a careful procedure is followed. Despite the marginal improvement, the alloyed high silicon steels typically suffered from worsening magnetic properties.

5. Processing of high silicon steel

Due to its brittle nature at room temperature, processing of high silicon steel using the conventional route is not possible. Multiple processing techniques have been developed to mitigate the brittleness problem, including special thermal mechanical processing (combination of hot/warm/cold rolling), rapid solidification, and deposition/ diffusion annealing. All these processes are intended to produce thin silicon steel strips that can be laminated for practical applications. A few important properties including coercive force, permeability, magnetic induction, and iron losses at various conditions are summarized in Fig. 13 at the end of this section.

5.1. Thermal mechanical processing

A series of thermal mechanical processing experiments were performed on Fe-6.5 wt%Si by various groups, such as Houbaert and Schneider's group [112–117], Lin's group [118–120], and others [78,95,121,122]. These processes were possible due to the avoidance of ordering, either by using high temperatures for hot rolling, or quenching prior to the cold rolling runs. Hot rolling of slabs has to be conducted above 1000 °C as the mean flow stress was found to significantly increase in high silicon steel when the temperature drops below 950 °C, but remains low above 1000 °C [116]. In practice, Yanez showed that after heating the slabs to 1150–1250 °C, hot rolling in four or nine passes with a total reduction of about 95% is possible with no major problems [116,113]. Cold rolling was only possible by prior accelerated cooling. With the right processing parameters, a final thickness of 0.4 mm was achieved by cold rolling [113]. However, cold-rolled samples can lose their ductility due to rapid domain growth, and any further rolling was not possible [113]. Industry prefers hot and cold rolling processes because of minimum changes to the current low silicon steel production lines.

Another rolling technique involves the use of powders and may be called direct powder rolling. In this technique, atomized iron powders and silicon powders are blended by ball milling and then subjected to rolling. This process merely shapes the powder compacts and re-agglomerates the powders into a thin strip. High-temperature annealing

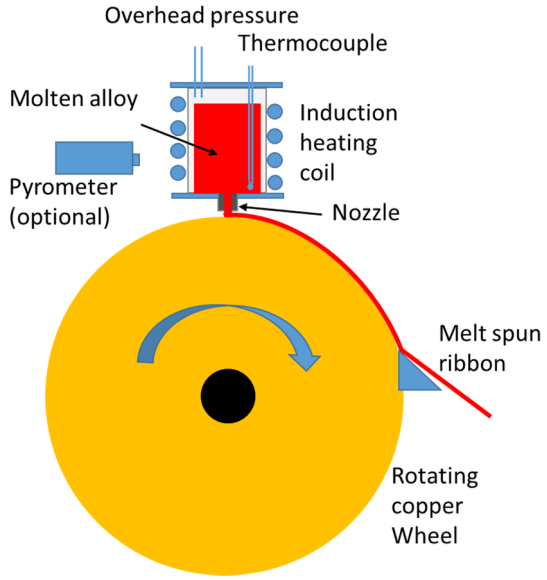

Fig. 11. Schematic depicting a typical set up of a melt-spinning system.

must be performed to alloy and homogenize the compacted strip. Li et al. produced 60-mm-wide and 0.2–0.35-mm-thick 6–6.5 wt% silicon steel strips by this method [123]. The annealed strip has a saturation induction value of 1.795 T, which is close to the theoretical value. However, the iron loss of the strip remains high. Although direct powder rolling effectively mitigates the brittleness issue, it brings in new problems such as contamination of powders, nonhomogeneous composition, and limitation in strip length.

5.2. Rapid solidification

The brittleness of high silicon steel originates from the B2 and $D0_3$ ordering. Rapid solidification techniques that surpass the ordered phases are thus widely studied for the production of high silicon steel.

One of the most widely used techniques in rapid solidification is melt spinning. In the melt spinning process, alloys are inductively melted in a crucible before being ejected onto a rotating wheel. Such a process directly produces continuous thin ductile strips with 10–100 μm thickness. A typical melt spinning setup is shown in Fig. 11. Melt spinning was used by Arai and Tsuya to produce 3.8 to 9.3 wt% silicon steel ribbons as early as 1980 [49]. Recent efforts by Lin's group [51,124] has brought the melt spinning of 6.5 wt% silicon steel one step further toward the production of large-scale ribbons with 25 mm width and 0.03 mm thickness. The melt-spun thin ribbon is ductile and can be bent 180° without cracking [65]. The magnetization of melt spun 6.5 wt % silicon steel is around 1.78 T; however, its coercivity can be large due to the small grain size and large strain [49,50]. Nevertheless, the coercivity may be reduced by high-temperature annealing, with 1200 °C for 35 min as the most suitable condition to produce the lowest coercivity [49]. Due to the presence of heat gradient from the ribbon wheel side and free side, the grains tend to grow columnarly along the ribbon thickness direction resulting in a certain degree of a ⟨1 0 0⟩ out-of-plane fiber texture [50,86]. This favorable texture makes melt-spun ribbons especially desirable for motor applications.

Many process parameters such as melt temperature, nozzle size, nozzle-to-wheel distance, wheel material, wheel speed, overheat, chamber gas, chamber pressure, and injection pressure must be closely controlled to obtain continuous high quality ribbons. Nickel-plated copper wheels were found to be the optimum wheel owing to their wetting behavior, whereas copper wheels could not produce well-shaped ribbons efficiently and steel wheel was found inefficient in

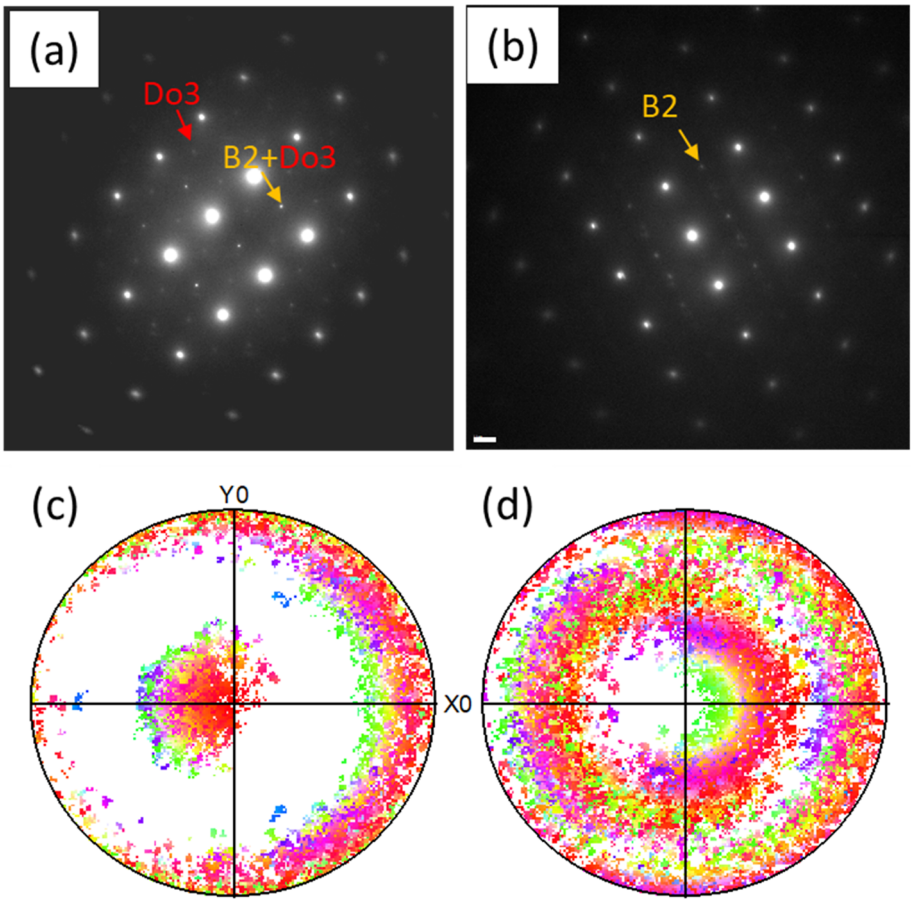

Fig. 12. (a), (b) TEM {1 1 0} zone diffraction patterns of 1 m/s and 30 m/s melt-spun ribbons, respectively. (c), (d) {1 0 0} and {1 1 0} pole figures obtained by electron backscatter diffraction (EBSD) technique showing ⟨0 0 1⟩ out-of-plane texture (with slight tilt with respect to the sample surface normal) of 30 m/s melt-spun ribbon.

cooling when processing large quantity of melt due to poor conduction [86]. Helium, compared to argon gas, created a less violent gas boundary layer, thus resulting in fewer air pockets and better ribbon shape [86]. Furthermore, the wheel speed affects the cooling rate and ribbon thickness [50], thereby can be used to control the degree of ordering [50], which in turn affects the mechanical properties and coercive force [50,109]. Electrical resistivity, however, remained constant for different wheel speeds [109]. Adjusting the wheel speed offers an opportunity to tune the texture and grain size as well as the ordering. Fig. 12 shows the difference in ordering at two different wheel speeds, and the ⟨0 0 1⟩ out-of-plane texture produced at a high wheel speed.

Melt spinning enables a direct production of ductile Fe-6.5 wt%Si thin sheet and can save a large amount of energy by avoiding the energy-consuming rolling processes. The wheel usually spins at 30 m/s, which implies a production speed of 30 m of sheet per second. The rapid quenching also minimized the oxidation, which eliminated the need for an acid wash, thus minimizing impact to environment. However, at its current stage, melt spinning can only offer a limited range of thickness (0.03–0.1 mm) and width (< 300 mm), and is now mainly used in laboratories to produce 6.5 wt% silicon steel in small scale (< 1 kg/batch).

As another rapid solidification technique, strip casting was explored for the processing of Fe-6.5 wt%Si steel. In the strip casting process, superheated molten metal is poured into a preheated tundish, where it is then flowed down through a nozzle onto water-cooled steel or copper rolls. A 1 to 2 mm thick cast strip is then air cooled to room temperature. Strip casting offers a high solidification rate and can produce strips with thicknesses close to that of the hot-rolled sheets. Wang's group recently conducted a series of studies on strip casting of silicon steel [87,88,125–132]. Strip casting of 3 wt% silicon steel was successful [87], and strip casting of 6.5 wt% high silicon steel was attempted [88,125]. However, rolling of the strip cast sheet remains challenging due to the lack of sufficient ductility [88,125]. The iron loss of 22–24 W/kg at 1 T and 400 Hz of the annealed strip [88,125] is high. The preferred ⟨0 0 1⟩ out-of-plane fiber texture is observed on the strip cast sample [87,127]. The degree of the texture was found to be dependent on the superheat, with high superheat resulting in elimination of equiaxed grains and improvement of the ⟨0 0 1⟩ fiber texture [87]. The preferred orientation randomizes after the subsequent rolling process. To retain the ⟨0 0 1⟩ fiber texture, an additional 1200 °C hot rolling process was found to be useful [88,125].

Strip casting allows the production of continuous strips several millimeters in thickness, and eliminates the hot rolling and acid wash step involved in the production of steel laminates. When needed, warm and cold rolling may be added to the strip casting line with ease. However, production of strip-cast high silicon steel with the desired thickness and sufficient ductility remains a challenge.

Though a desirable texture can be generated via various processing techniques, the microstructure is likely to be randomized during subsequent high-temperature annealing which is essential to achieve good magnetic properties. One way of maintaining the preferred texture is by directional recrystallization, wherein the sample is passed through a hot zone with a temperature gradient to achieve directional recrystallization. This process favors the growth of columnar grains, thereby inducing a preferred orientation. Various reports on directional solidification/recrystallization are available in the literature [61,89–91,133,134]. For example, {1 1 0} ⟨1 1 1⟩ and {1 1 1} ⟨1 1 0⟩ texture components were introduced to Fe-6.5 wt%Si high silicon steel using a 1150 °C directional recrystallization process [89]. The coercivity of the obtained sample in the direction 60° away from the growth direction is remarkable, reaching 13.9 A/m, which is the result of oriented grains and a large grain size. The processing parameters such as hot zone temperature [90], growth rate [90], and directional solidification rates, i.e., the specimen-withdrawing velocity [90] can be tuned to optimize the texture.

5.3. Deposition/diffusion annealing

The deposition/diffusion annealing approach utilizes ductile low silicon steel as feedstock. A higher silicon content is achieved through surface deposition techniques of high silicon containing chemicals. Diffusion annealing is then performed to achieve uniform distribution of silicon. The deposition method varies, including chemical vapor deposition (CVD), hot dipping, physical vapor deposition (PVD), and spray forming.

NKK Corporation, now a part of JFE steel, pioneered the production of gradient 6.5 wt% Si steel using CVD approach [35,95,135]. In their process, Si is deposited on the surface of 3 wt% Si steel sheet by passing silicon tetrachloride ($SiCl_4$) gas over and then allowing Si to diffuse into the bulk at 1200 °C [136]. The following chemical reaction occurs during the diffusion process.

$$SiCl_4 + 5Fe \rightarrow Fe_3Si + 2FeCl_2 \quad (5)$$

Such a CVD process has some drawbacks such as the limitation of sheet thickness and high environmental impact due to the use of harmful $SiCl_4$. The health effects upon exposure to $SiCl_4$ have been mentioned in literature [137,138] and media [139].

The hot dipping and diffusion annealing route to producing 6.5 wt% gradient silicon steel was introduced by Ros-Yanez et al. [116,140]. In this method, 0.35-mm-thick 3.2 wt% silicon steel was dipped into an Al-Si hypereutectic bath (25 wt% Si) at 800 °C to achieve a multilayer Fe-containing intermetallics, which was then annealed at 1250 °C for 30 min to achieve homogeneous Si and Al concentrations of up to 6.5 wt % and 4.5 wt%, respectively. The sample immersed for 100 s and annealed at 800 °C for 60 s showed a power loss of 33.57 W/kg at 1 T and 400 Hz; further annealing at 1250 °C for 30 min resulted in W10/400 of 10.56 W/kg. This method is similar to the JFE steel CVD process and may have potential for mass production. However, the introduction of aluminum is unavoidable, which may adversely affect the magnetic properties such as magnetization and magnetostriction.

PVD methods have been investigated such as electron beam PVD [141] or magnetron sputtering deposition. However, the formation of pores [141] or porous interfaces [142] remains a problem and adversely affects the magnetic properties [141]. While the application of PVD method may be viable for small samples, the mass production of wide sheet is challenging.

Spray forming uses a carrier gas such as Ar to spray atomize liquid metal Si onto a rotating iron substrate [121] or strip [143]. Then, the samples are homogenized at 1100 °C for 10 h [121] followed by rolling to reduce the strip to thinner gauges. To increase the ductility during the rolling process, Al was added to the cold spraying process [144–146], which improved the ductility due to the avoidance of B2 ordering owing to the presence of Al; however, the formation of inclusions impaired the magnetic properties. A recent effort by Cava et al. [147–149] focused on co-spraying Fe-3.5 wt%Si + 3 wt% Si on a 1020 steel substrate. However, the presence of oxide particles in the final microstructure remains a problem.

5.4. Comparison of magnetic properties

The magnetic properties of 6.5 wt% silicon steel is plotted in Fig. 13 [35,47,78,88,95,118,120,124,125,140,142]. The iron losses are dependent on the thickness, except at a low frequency of 50 Hz. The low frequency loss W10/50 has a significant contribution from the hysteresis loss, and thus, the thickness dependence is not prominent, and the typical losses range from 0.5 W/kg to 0.7 w/kg for all the methods referenced. Eddy current loss makes a larger contribution when testing at higher frequency. The dependence on thickness at high frequencies is thus more significant, with thinner thicknesses generating much lower iron losses.

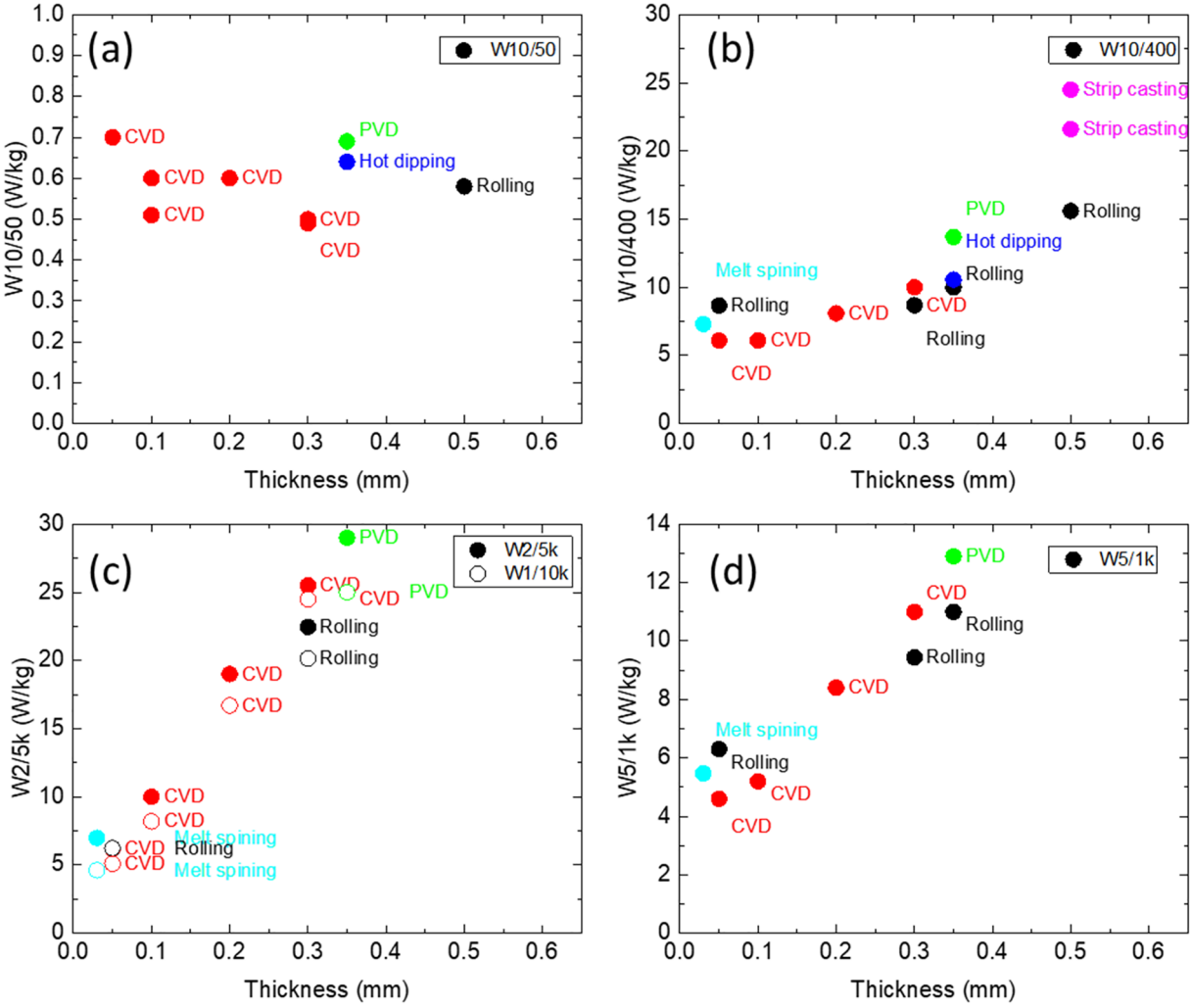

Fig. 13. Comparison of AC magnetic iron losses of Fe-6.5 wt%Si steel produced by different methods tested at different conditions [35,47,78,88,95,118,120,124,125,140,142].

6. Application

Soft magnetic materials are extensively used in the fields of electricity conversion, electric machines, sensors, EMI prevention, and electronic components. This section provides a brief introduction of the potential applications of high silicon steel and the desired materials properties.

6.1. Electricity conversion

Electricity are frequently converted between AC and DC, and between different voltages and frequencies. Devices such as transformers, inverters, converters, and frequency modulators accomplish the conversion using soft magnetic materials [150]. Transformers are used to alter the AC voltages. Based on the operating frequency, the transformers can be classified as 50/60 Hz distribution transformers [151,152], 400 Hz transformers [25], and high-frequency (audio/radio) transformers [31,40]. While 50/60 Hz transformers are extensively used in residential applications, 400 Hz transformers are popular in aviation industry [153] and military applications [154] where high power density is desired. Inverters convert DC power to AC power, and are primarily used by solar power systems, fuel cell power systems, uninterruptible power supplies [155], and electric vehicle motor drives [154,156]. Converters are used to convert AC to DC for battery charging, and frequency modulators which modifies frequency.

For applications in the frequency range of 0–10^2 Hz, cost is the primary consideration. While high saturation magnetization and high permeability are highly desired, high electrical resistivity (> 50 μΩ-cm) is also preferred but not as critical. In addition, low coercivity and low hysteresis are required for a low power loss. In contrast, for applications in the frequency range of 10^2–10^{10} Hz, high electrical resistivity is necessary. The requirements also include high permeability and low power loss [157]. High silicon steel (6.5 wt% Si) satisfies all the requirements for low to medium frequency applications (up to 1 kHz) and has become a candidate for applications in high-frequency (up to 15 kHz [158]) inductors in the automotive, aerospace, and stationary power generation industries [159]. Currently, 6.5 wt% silicon steel from JFE steel prepared by the CVD process are used as the core materials of the inductors of 15 kHz buck-boost converters in Toyota Prius hybrid electric vehicles (HEVs) [158]. Other 6.5 wt% silicon steel products such as MEGA flux from Chang Sung Corporation [160], XFLUX from Magnetics Inc. [161], Fluxsan from Micrometals Inc. [162], and DF series from Hengdian Group [163] are also commercially available for inductor applications [164]. The performances of Fe-6.5 wt%Si powder core, ferrite core, and nanocrystalline core for the inductor of a buck-boost converter were compared by You et al. [158]. And Fe-6.5 wt%Si powder core was found favorable owing to its high saturation, low core losses at 10 KHz, high thermal stability, low acoustic noise, and more importantly, low cost [158].

6.2. Electric machine

Electric machine has two variations, one is power generator and the other is electric motor. The rotating magnetic field between a rotor and a stator leads to the conversion of mechanical energy into electrical energy for generators and the reverse conversion for motors. The application of advanced soft magnetic materials to rotors and stators is the key for high efficiency motors which operates at high frequencies to meet the trend of system miniaturization and cost reduction [99,165–168]. For electric machines to achieve their best performance, high magnetization, high permeability, low coercivity, high electrical resistivity, and high Curie temperatures are indispensable magnetic properties [169].

Non-oriented silicon steel finds many applications in electric vehicle. Its application includes traction motors, power steering motor, wind-shield wiper motor, seat adjuster motor, fuel pump, HVAC compressor and fans, window life motor, and electrical turbocharger motors. The 6.5 wt% Si steel is more attractive due to its low raw material cost, near-zero magnetostriction, and low iron losses at higher frequencies [99].

6.3. Sensors

Sensors convert energy from one form into another to detect, measure, and analyze the source signal. The demand for high-performance and cost-effective sensors is rapidly growing [170]. Various magnetic effects are employed by sensors, such as electromagnetic effect, Hall effect, magnetoresistive effect, magnetoelastic effect, and giant magnetoimpedance effect [171]. These effects are used in a number of devices such as magnetic field sensors [172], stress/strain sensors [170,173,174], current sensors [175], temperature sensors [176,177], and light sensors [178]. In general, a sensor material should have low coercivity, temperature-stable permeability, and high electrical resistivity [179]. However, individual sensors may have different requirements due to the nature of the magnetic effects being utilized.

Magnetic sensors are widely used in the automotive industries such as anti-lock brake system sensor rings, pump angle sensors, ignition system pulse generators and rotational speed sensors, power steering system rotation and torque sensors, and electronic gearbox control system input and output speed sensors. [180]. Currently, these sensors use ferrite, stainless steel, or iron. However, these can all be the potential applications of the 6.5 wt% silicon steel, which is capable of delivering lower losses. Particularly, the 6.5 wt% silicon steels may be a direct replacement for silicon steels in which are used in high-frequency pulsed current step motor sensors, where these sensors are used to provide electronic control of the valve openings [180].

6.4. Electromagnetic interference (EMI) prevention

EMI is the electromagnetic disturbance that degrades the performance of electrical circuits [181]. With the ever-increasing utilization of electronic devices in our daily lives, EMI prevention have been attracting great interests for devices protection. One form of protection is the common mode chokes, which operate by acting as a low-impedance wire to pass the desired signal and as a high-impedance inductor to block high-frequency noise [182]. Electromagnetic field shielding prevents EMI as well [183,184]. It could be used either for passive shielding by drawing the magnetic field into itself, or for active shielding by generating a field to eliminate the external field. These applications largely pertain to the aviation and telecommunication industries [185].

The materials used for EMI applications require a high initial permeability and remain stable in frequencies up to 10 MHz, and should maintain high impedance within a wide frequency range and at high operating temperatures [186]. The currently popular EMI materials are Ferrites [187], amorphous, nanocrystalline alloys, and iron-nickel alloys [188]. However, with the increasing demands for higher flux densities [189], materials with high magnetic saturation and high electrical resistivity would be necessary. High silicon steel could be a viable candidate if its electrical resistivity is further enhanced by forming a composite with non-conductive coating materials.

6.5. Electronic components

Soft magnetic materials are widely employed in electronic components. Among them, applications in the fields of data storage and telecommunication are of tremendous significance in the current information age. The magnetic read/write head material for data storage is a good representation in this field [190,191]. These materials must have high magnetization, high initial permeability, high mechanical hardness, high wear resistance, and near-zero magnetostriction [31]. Telecommunication applications deal with transmitting information via the conversion between electric current and electromagnetic wave [169], which requires a low core loss at a high frequency (MHz to GHz) [192]. Additionally, numerous electronic components take advantage of soft magnetic materials to perform their functions, such as circulators, isolators, limiters, phase shifters [182], pulse transformers [193], inductors [194,195], switches [196], and amplifiers [183]. Examples of soft magnetic materials in this category may include dimmer switches, contact plates, heater valves, relay armatures, and gas security valve cores [180]. For parts that require high resistivity and high permeability, silicon steel is the usual choice, such as printer heads in the impact printers used in automated teller machines [180].

6.6. Others

In addition to magnetic properties, soft magnetic materials demonstrate other advantageous properties. For instance, a low Young's modulus allows soft magnetic materials to be used as automobile valve springs [193]. Similarly, high stiffness is the optimal property for the materials of certain sporting goods, such as golf clubs, baseball bats, snowboards, and fishing equipment [197]. Soft magnetic materials are extensively utilized in chemical and medical applications as well [198,199].

7. Summary

Soft magnetic materials find wide applications in today's electric and electronic world. While soft magnetic materials enables energy conversion, they consumes a significant amount of energy during the process due to the iron loss. To conserve energy and meet the increasing demand for high-frequency operation, the iron loss of soft magnetic materials needs to be minimized. High silicon steel, more specifically, 6.5 wt% silicon steel possesses high electrical resistivity, high saturation magnetization, zero magnetostriction, and low raw material cost, which make it a promising candidate for mid-frequency applications. However, 6.5 wt% silicon steel is brittle due to the formation of ordered phases, and cannot be processed using the economical cold rolling method. A number of processing techniques such as thermal mechanical processing, rapid solidification, and deposition/diffusion annealing have been investigated for manufacturing ductile 6.5 wt% silicon steel sheet. These methods have drawbacks including high cost, limitations in width and thickness, and adverse environmental impact. To enable the wide application of 6.5 wt% silicon steel, these drawbacks, in particular, the overall processing cost must be thoroughly addressed.

Fe-6.5 wt%Si steel can be used in various forms such as wound tape, stacked laminates, or powders/flakes compacts. It is important to obtain ductile Fe-6.5 wt%Si sheet by suppressing the embrittling ordering phases, as ductility is needed for the subsequent mechanical processes such as spooling or stamping. The ability to prepare sufficiently wide sheet is critical, as it is the basis for large laminates for electric motors. It should be noted that the ultimate goal is to achieve the optimum

magnetic property with the material in its final form. In most cases, the rapidly solidified disordered Fe-6.5 wt%Si steel with fine-grains cannot be directly used because the ordered B2 and $D0_3$ phases that are responsible for better magnetic properties are missing [62]. Annealing is required to call back these phases, relieve stress and increase grain size, albeit additional annealing process inevitably imposes processing complexity.

Acknowledgments

This work was financially supported by the U.S. Department of Energy, Office of Energy Efficiency and Renewable Energy (EERE) under the Award Number EE0007794. The research was performed at Iowa State University and at Ames Laboratory, which is operated for the U.S. Department of Energy by Iowa State University under the contract number DE-AC02-07CH11358.

References

[1] B.D. Cullity, C.D. Graham, Introduction to Magnetic Materials, Wiley-IEEE Press, 2008.
[2] U.S. Department of Energy, Premium Efficiency Motor Selection and Application Guide. https://www.energy.gov/sites/prod/files/2014/04/f15/amo_motors_handbook_web.pdf, 2014, (accessed 11/28/2018).
[3] Teknomotor Product Catalog http://www.teknomotor.com/pdf/catalogo.pdf, (accessed 11/28/2018).
[4] The Scale up of Wide Bandgap Power Semiconductor Technology and Power Electronics. https://www.nist.gov/document-2981, (accessed 11/28/2018).
[5] O. Fischer, J. Schneider, Influence of deformation process on the improvement of non-oriented electrical steel, J. Magn. Magn. Mater. 254–255 (2003) 302–306.
[6] F. Fiorillo, Characterization and Measurement of Magnetic Materials, Academic Press, 2004.
[7] M.F. Littmann, Iron and silicon-iron alloys, IEEE Trans. Magn. MAG7 (1) (1971) 48–60.
[8] H. Shimanaka, Y. Ito, K. Matsumara, B. Fukuda, Recent development of non-oriented electrical steel sheets, J. Magn. Magn. Mater. 26 (1) (1982) 57–64.
[9] Super CoreTM Electrical steel sheets for high-frequency application, JFE Steel Corporation. http://www.jfe-steel.co.jp/en/products/electrical/catalog/f1e-002.pdf, (accessed 11/28/2018).
[10] S. Constannides, Energy Savings with Thin Gauge Silicon-Iron, Arnold Magnetic Technologies. http://www.arnoldmagnetics.com/wp-content/uploads/2017/10/Energy-Savings-with-Thin-Gauge-Silicon-Iron-thingagesife_100213c_final-ppr.pdf, (accessed 11/28/2018).
[11] Y. Chen, V.G. Harris, Magnetic grain boundary engineered ferrite core materials, Google Patents, 2015.
[12] Y. Ushigami, M. Mizokami, M. Fujikura, T. Kubota, H. Fujii, K. Murakami, Recent development of low-loss grain-oriented silicon steel, J. Magn. Magn. Mater. 254–255 (2003) 307–314.
[13] N. Leuning, S. Steentjes, K. Hameyer, Effect of grain size and magnetic texture on iron-loss components in NO electrical steel at different frequencies, J. Magn. Magn. Mater. 469 (2019) 373–382.
[14] S. Washko, E. Choby, Evidence for the effectiveness of stress coatings in improving the magnetic properties of high permeability 3% Si-Fe, IEEE Trans. Magn. 15 (6) (1979) 1586–1591.
[15] E. Beyer, L. Lahn, C. Schepers, T. Stucky, The influence of compressive stress applied by hard coatings on the power loss of grain oriented electrical steel sheet, J. Magn. Magn. Mater. 323 (15) (2011) 1985–1991.
[16] A.J. Moses, Effects of applied stress on the magnetic-properties of high permeability silicon-iron, IEEE Trans. Magn. 15 (6) (1979) 1575–1579.
[17] L. Kestens, S. Jacobs, Texture Control During the Manufacturing of Nonoriented Electrical Steels, Texture, Stress, and Microstructure 2008(Article ID 173083), 2008. p. 9.
[18] A. Schoppa, J. Schneider, C.D. Wuppermann, Influence of the manufacturing process on the magnetic properties of non-oriented electrical steels, J. Magn. Magn. Mater. 215–216 (2000) 74–78.
[19] W.F. Barrett, W. Brown, R.A. Hadfield, Electrical conductivity and magnetic permeability of various alloys of Fe, Sci. Trans. Roy. Dublin Soc. 7 (1900) 67–126.
[20] H.D. Arnold, G.W. Elmen, Permalloy, a new magnetic material of very high permeability, Bell Syst. Tech. J. 2 (3) (1923) 101–111.
[21] J.L. Snoek, Magnetic Core, 1948.
[22] P. Duwez, S.C.H. Lin, Amorphous ferromagnetic phase in iron-carbon-phosphorus alloys, J. Appl. Phys. 38 (10) (1967) 4096–4097.
[23] K.I. Arai, N. Tsuya, K. Ohmori, H. Shimanaka, T. Miyazaki, Rapidly quenched ribbon-form silicon-iron alloy with high silicon concentration, J. Magn. Magn. Mater. 15–8(JAN-) (1980) 1425–1426.
[24] Y. Yoshizawa, S. Oguma, K. Yamauchi, New Fe-based soft magnetic alloys composed of ultrafine grain structure, J. Appl. Phys. 64 (10) (1988) 6044–6046.
[25] J.M. Coey, Magnetism and Magnetic Materials, Cambridge University Press, 2010.
[26] J.M. Silveyra, E. Ferrara, D.L. Huber, T.C. Monson, Soft magnetic materials for a sustainable and electrified world, Science 362 (6413) (2018).
[27] J.D. Adam, L.E. Davis, G.F. Dionne, E.F. Schloemann, S.N. Stitzer, Ferrite devices and materials, IEEE Trans. Microw. Theory Tech. 50 (3) (2002) 721–737.
[28] V.G. Harris, A. Geiler, Y. Chen, S.D. Yoon, M. Wu, A. Yang, Z. Chen, P. He, P.V. Parimi, X. Zuo, C.E. Patton, M. Abe, O. Acher, C. Vittoria, Recent advances in processing and applications of microwave ferrites, J. Magn. Magn. Mater. 321 (14) (2009) 2035–2047.
[29] F.J.G. Landgraf, Nonoriented electrical steels, JOM 64 (7) (2012) 764–771.
[30] A. Krings, A. Boglietti, A. Cavagnino, S. Sprague, Soft magnetic material status and trends in electric machines, IEEE Trans. Ind. Electron. 64 (3) (2017) 2405–2414.
[31] M.E. McHenry, M.A. Willard, D.E. Laughlin, Amorphous and nanocrystalline materials for applications as soft magnets, Prog. Mater Sci. 44 (4) (1999) 291–433.
[32] G. Herzer, Modern soft magnets: amorphous and nanocrystalline materials, Acta Mater. 61 (3) (2013) 718–734.
[33] E. Theisen, Development of new amorphous and nanocrystalline magnetic materials for use in energy-efficient devices, MRS Adv. 2 (56) (2017) 3409–3414.
[34] R.M. Bozorth, Ferromagnetism, Van Nostrand, New York, 1951.
[35] H. Haiji, K. Okada, T. Hiratani, M. Abe, M. Ninomiya, Magnetic properties and workability of 6.5% Si steel sheet, J. Magn. Magn. Mater. 160 (1996) 109–114.
[36] G. Herzer, Soft Magnetic Materials—Nanocrystalline Alloys, Handbook of Magnetism and Advanced Magnetic Materials, John Wiley & Sons, Ltd, 2007.
[37] O. Gutfleisch, M.A. Willard, E. Bruck, C.H. Chen, S.G. Sankar, J.P. Liu, Magnetic materials and devices for the 21st century: stronger lighter, and more energy efficient, Adv. Mater. 23 (7) (2011) 821–842.
[38] M.A. Willard, D.E. Laughlin, M.E. McHenry, D. Thoma, K. Sickafus, J.O. Cross, V.G. Harris, Structure and magnetic properties of (Fe0.5Co0.5)88Zr7B4Cu1 nanocrystalline alloys, J. Appl. Phys. 84 (12) (1998) 6773–6777.
[39] A. Makino, Nanocrystalline soft magnetic Fe-Si-B-P-Cu alloys with high B of 1.8–1.9T contributable to energy saving, IEEE Trans. Magn. 48 (4) (2012) 1331–1335.
[40] D. Jiles, Introduction to Magnetism and Magnetic Materials, third ed., CRC Press, 2015.
[41] J. Tangudu, G. Ouyang, J. Cui, Trade studies for a manganese bismuth based surface permanent magnet machine, IEEE Transp. Electrif. Conf. Expo (ITEC) 2018 (2018) 600–605.
[42] E. Gumlich, D.I.P. Goerens, Magnetic properties of iron-carbon and iron-silicon alloys, 1912.
[43] C. Albert, On the magnetic properties of silicon iron (Stalloy) in alternating magnetic fields of low value, Proc. Phys. Soc. London 32 (1) (1919) 232.
[44] P. Beckley, E. Institution of Electrical, Electrical Steels for Rotating Machines, Institution of Electrical Engineers, 2002.
[45] B. Verbrugge, D.C. Jiles, Core loss reduction in electrical steels through materials processing, J. Appl. Phys. 85 (8) (1999) 4895–4897.
[46] Y. Yi, Z. Zhou, Z. Wang, S. Jiang, W. Huang, Si-steel thin-strip prepared by twin-roll continuous casting, Surf. Review. Lett. 18 (03n04) (2011) 97–102.
[47] H. Ninomiya, Y. Tanaka, A. Hiura, Y. Takada, Magnetostriction and applications of 6.5% Si steel sheet, J. Appl. Phys. 69 (8) (1991) 5358–5360.
[48] X.F. Bi, Y. Tanaka, K. Sato, Effect of microstructure on the magnetic properties of 6.5% Si Fe alloy, J. Magn. Magn. Mater. 112 (1) (1992) 189–191.
[49] K.I. Arai, N. Tsuya, Ribbon-form silicon-iron alloy containing around 6.5 percent silicon, IEEE Trans. Magn. 16 (1) (1980) 126–129.
[50] G. Ouyang, B. Jensen, W. Tang, K. Dennis, C. Macziewski, S. Thimmaiah, Y. Liang, J. Cui, Effect of wheel speed on magnetic and mechanical properties of melt spun Fe-6.5 wt.% Si high silicon steel, AIP Adv. 8 (5) (2018) 056111.
[51] Y.F. Liang, S. Wang, H. Li, Y.M. Jiang, F. Ye, J.P. Lin, Fabrication of Fe-6.5 wt%Si ribbons by melt spinning method on large scale, Adv. Mater. Sci. Eng. 2015 (2015) 296197.
[52] M. Miyazaki, M. Ichikawa, T. Komatsu, K. Matusita, Formation and electronic state of Do3-type ordered structure in sputtered Fe-Si thin-films, J. Appl. Phys. 71 (5) (1992) 2368–2374.
[53] P. Arató, I. Bóc, T. Gróf, Effect of composition on the loss of non-oriented medium silicon electric steels, J. Magn. Magn. Mater. 41 (1) (1984) 53–55.
[54] C.-K. Hou, Effect of silicon on the loss separation and permeability of laminated steels, J. Magn. Magn. Mater. 162 (2) (1996) 280–290.
[55] T. Kan, Y. Ito, H. Shimanaka, Magnetic properties of roller-quenched high silicon steel ribbons, J. Magn. Magn. Mater. 26 (1) (1982) 127–129.
[56] W.E. Ruder, New magnetic materials, Proc. IRE 30 (10) (1942) 437–440.
[57] J.S. Shin, J.S. Bae, H.J. Kim, H.M. Lee, T.D. Lee, E.J. Lavernia, Z.H. Lee, Ordering-disordering phenomena and micro-hardness characteristics of B2 phase in Fe-(5–6.5%)Si alloys, Mater. Sci. Eng. A 407 (1–2) (2005) 282–290.
[58] P.R. Swann, L. Grånäs, B. Lehtinen, The B2 and DO3 ordering reactions in iron-silicon alloys in the vicinity of the curie temperature, Metal Sci. 9 (1) (1975) 90–97.
[59] D. Ruiz, T.R. Yanez, G.J. Cuello, R.E. Vandenberghe, Y. Houbaert, Order in Fe-Si alloys: a neutron diffraction study, Phys. B Condens. Matter. 385 (2006) 578–580.
[60] G.E. Dieter, Mechanical Metallurgy, McGraw-Hill, New York, 1961.
[61] H.D. Fu, Q. Yang, Z.H. Zhang, J.X. Xie, Effects of precipitated phase and order degree on bending properties of an Fe-6.5 wt%Si alloy with columnar grains, J. Mater. Res. 26 (14) (2011) 1711–1718.
[62] K. Narita, M. Enokizono, Effect of ordering on magnetic properties of 6.5-percent silicon-iron alloy, Magn. IEEE Trans. 15 (1) (1979) 911–915.
[63] K. Raviprasad, K. Aoki, K. Chattopadhyay, The nature of dislocations and effect of order in rapidly solidified Fe–(5.5–7.5)wt.%Si alloys, Mater. Sci. Eng. A 172 (1) (1993) 125–135.
[64] Z.H. Zhang, W.P. Wang, H.D. Fu, J.X. Xie, Effect of quench cooling rate on residual stress, microstructure and mechanical property of an Fe-6.5Si alloy, Mater. Sci. Eng. A Struct. Mater. Prop. Microstruct. Process. 530 (2011) 519–524.

[65] S. Cui, G. Ouyang, T. Ma, C.R. Macziewski, V.I. Levitas, L. Zhou, M.J. Kramer, J. Cui, Thermodynamic and kinetic analysis of the melt spinning process of Fe-6.5 wt.% Si alloy, J. Alloy. Compd. 771 (2019) 643–648.
[66] B. Viala, J. Degauque, M. Fagot, M. Baricco, E. Ferrara, F. Fiorillo, Study of the brittle behaviour of annealed Fe-6.5 wt%Si ribbons produced by planar flow casting, Mater. Sci. Eng., A 212 (1) (1996) 62–68.
[67] X. Wang, H. Liu, H. Li, Z. Liu, Effect of cooling rate on order degree of 6.5 wt.% Si electrical steel after annealing treatment, IEEE Trans. Magn. 51 (11) (2015) 1–4.
[68] H.D. Fu, Z.H. Zhang, Q. Yang, J.X. Xie, Strain-softening behavior of an Fe–6.5 wt% Si alloy during warm deformation and its applications, Mater. Sci. Eng., A 528 (3) (2011) 1391–1395.
[69] F. Pfeifer, C. Radeloff, Soft magnetic Ni-Fe and Co-Fe alloys – some physical and metallurgical aspects, J. Magn. Magn. Mater. 19 (1) (1980) 190–207.
[70] G. Herzer, Grain size dependence of coercivity and permeability in nanocrystalline ferromagnets, IEEE Trans. Magn. 26 (5) (1990) 1397–1402.
[71] C.P. Steinmetz, On the law of hysteresis, Trans. Am. Inst. Electr. Eng. IX (1) (1892) 1–64.
[72] J. Reinert, A. Brockmeyer, R.W.A.A.D. Doncker, Calculation of losses in ferro- and ferrimagnetic materials based on the modified Steinmetz equation, IEEE Trans. Ind. Appl. 37 (4) (2001) 1055–1061.
[73] L. Jieli, T. Abdallah, C.R. Sullivan, Improved calculation of core loss with non-sinusoidal waveforms, in: Conference Record of the 2001 IEEE Industry Applications Conference. 36th IAS Annual Meeting (Cat. No.01CH37248), 2001, vol. 4. pp. 2203–2210.
[74] K. Venkatachalam, C.R. Sullivan, T. Abdallah, H. Tacca, Accurate prediction of ferrite core loss with nonsinusoidal waveforms using only Steinmetz parameters, 2002 IEEE Workshop on Computers in Power Electronics, 2002. Proceedings, 2002, pp. 36–41.
[75] G.E. Fish, Soft, magnetic materials, Proc. IEEE 78 (6) (1990) 947–972.
[76] C.D. Graham, Physical origin of losses in conducting ferromagnetic materials (invited), J. Appl. Phys. 53 (11) (1982) 8276–8280.
[77] R.H. Pry, C.P. Bean, Calculation of the energy loss in magnetic sheet materials using a domain model, J. Appl. Phys. 29 (3) (1958) 532–533.
[78] J. Qin, P. Yang, W. Mao, F. Ye, Effect of texture and grain size on the magnetic flux density and core loss of cold-rolled high silicon steel sheets, J. Magn. Magn. Mater. 393 (2015) 537–543.
[79] J. Füzer, Z. Birčáková, A. Zelenáková, P. Hrubovčák, P. Kollár, M. Predmerský, J. Hunady, Investigation of total losses of non-oriented electrical steels, Acta Phys. Polonica-Ser. A Gen. Phys. 118 (5) (2010) 1018.
[80] M.F. de Campos, J.C. Teixeira, F.J.G. Landgraf, The optimum grain size for minimizing energy losses in iron, J. Magn. Magn. Mater. 301 (1) (2006) 94–99.
[81] Y. Oda, Y. Tanaka, A. Chino, K. Yamada, The effects of sulfur on magnetic properties of non-oriented electrical steel sheets, J. Magn. Magn. Mater. 254 (2003) 361–363.
[82] H. Shimanaka, T. Irie, K. Matsumura, H. Nakamura, A new non-oriented silicon-steel with texture of [100] (Ovw), J. Magn. Magn. Mater. 19 (1–3) (1980) 63–64.
[83] M. Komatsubara, K. Sadahiro, O. Kondo, T. Takamiya, A. Honda, Newly developed electrical steel for high-frequency use, J. Magn. Magn. Mater. 242 (2002) 212–215.
[84] K.N. Kim, L.M. Pan, J.P. Lin, Y.L. Wang, Z. Lin, G.L. Chen, The effect of boron content on the processing for Fe–6.5wt% Si electrical steel sheets, J. Magn. Magn. Mater. 277 (3) (2004) 331–336.
[85] N.P. Goss, Electrical sheet and method and apparatus for its manufacture and test, Google Patents, 1934.
[86] Y. Sato, T. Sato, Y. Okazaki, Production and properties of melt-spun Fe-6.5wt.%Si ribbons, Mater. Sci. Eng. 99 (1988) 73–76.
[87] H. Liu, Z. Liu, C. Li, G. Cao, G. Wang, Solidification structure and crystallographic texture of strip casting 3wt% Si non-oriented silicon steel, Mater. Charact. 62 (5) (2011) 463–468.
[88] H.-T. Liu, Z.-Y. Liu, Y.-Q. Qiu, Y. Sun, G.-D. Wang, Microstructure, texture and magnetic properties of strip casting Fe–6.2wt%Si steel sheet, J. Mater. Process. Technol. 212 (9) (2012) 1941–1945.
[89] Z.W. Zhang, G. Chen, H. Bei, F. Ye, G.L. Chen, C.T. Liu, Improvement of magnetic properties of an Fe-6.5 wt % Si alloy by directional recrystallization, Appl. Phys. Lett. 93 (19) (2008).
[90] Z.W. Zhang, G. Chen, H.B. Bei, F. Li, F. Ye, G.L. Chen, C.T. Liu, Directional re-crystallization and microstructures of an Fe-6.5 wt%Si alloy, J. Mater. Res. 24 (8) (2009) 2654–2660.
[91] H.D. Fu, Z.H. Zhang, Y.B. Jiang, J.X. Xie, Improvement of magnetic properties of an Fe–6.5 wt.% Si alloy by directional solidification, Mater. Lett. 65 (9) (2011) 1416–1419.
[92] H.C. Fiedler, R.H. Pry, Effect of magnetic annealing on the properties of (110) [001] oriented 3 14% silicon-iron strip, J. Appl. Phys. 30 (4) (1959) S109–S110.
[93] J.F. Dillinger, R.M. Bozorth, Heat treatment of magnetic materials in a magnetic field – I. Survey of iron-cobalt-nickel alloys, Phy. J Gen. Appl. P6 (1) (1935) 279–284.
[94] M. Goertz, Iron-silicon alloys heat treated in a magnetic field, J. Appl. Phys. 22 (7) (1951) 964–965.
[95] M. Abe, Y. Takada, T. Murakami, Y. Tanaka, Y. Mihara, Magnetic-properties of commercially produced Fe-6.5wt-percent Si sheet, J. Mater. Eng. 11 (1) (1989) 109–116.
[96] Y. Inokuti, Grain oriented silicon steel sheet with a ceramic film characterized by ultra-low iron loss, Vacuum 47 (6–8) (1996) 857–862.
[97] T. Iuchi, S. Yamaguchi, T. Ichiyama, M. Nakamura, T. Ishimoto, K. Kuroki, Laser processing for reducing core loss of grain oriented silicon steel, J. Appl. Phys. 53 (3) (1982) 2410–2412.
[98] H. Kobayashi, K. Kuroki, E. Sasaki, M. Iwasaki, N. Takahashi, Heatproof domain refining method using combination of local strain and heat-treatment for grain oriented 3-percent Si-Fe, Phys. Scripta T 24 (1988) 36–41.
[99] Y. Oda, M. Kohno, A. Honda, Recent development of non-oriented electrical steel sheet for automobile electrical devices, J. Magn. Magn. Mater. 320 (20) (2008) 2430–2435.
[100] K.C. Lin, E.E. Zook, A desirable material for transformer cores, J. Mater. Eng. 11 (1) (1989) 117–121.
[101] Y. Kurosaki, H. Mogi, H. Fujii, T. Kubota, M. Shiozaki, Importance of punching and workability in non-oriented electrical steel sheets, J. Magn. Magn. Mater. 320 (20) (2008) 2474–2480.
[102] H. Shokrollahi, K. Janghorban, Soft magnetic composite materials (SMCs), J. Mater. Process. Technol. 189 (1) (2007) 1–12.
[103] H. Miura, H. Kang, Application of metal injection moulding to soft magnetic materials, Powder Metall. 56 (1) (2013) 38–45.
[104] Z.Y. Wu, X. Fan, J. Wang, G.Q. Li, Z.H. Gan, Z. Zhang, Core loss reduction in Fe-6.5 wt.%Si/SiO2 core-shell composites by ball milling coating and spark plasma sintering, J. Alloys Compd. 617 (2014) 21–28.
[105] X.A. Fan, Z.Y. Wu, G.Q. Li, J. Wang, Z.D. Xiang, Z.H. Gan, High, resistivity and low core loss of intergranular insulated Fe-6.5 wt.%Si/SiO2 composite compacts, Mater. Des. 89 (2016) 1251–1258.
[106] J. Cui, G. Ouyang, B. Jensen, K. Dennis, B. Cui, Near net shape bulk laminated silicon iron electric steel for improved electric resistance and low high frequency loss, ISURF 04708, 2017.
[107] H. Seifert, M. Jurisch, J. Tobisch, C.G. Oertel, Mechanical properties of Fe-4.5-6wt.%Si double roller ribbons, Mater. Sci. Eng. A 133 (1991) 292–296.
[108] R.W. Cahn, P. Haasen, Physical metallurgy, North-Holland Phys. Pub. (1983).
[109] K. Narita, N. Teshima, Y. Mori, M. Enokizono, Recent researches on high silicon-iron alloys, IEEE Trans. Magn. 17 (6) (1981) 2857–2862.
[110] A.M. Glezer, I.V. Maleeva, A.I. Zakharov, Influence of alloy elements on the plasticity of high-silicon iron, Met. Sci. Heat Treat+ 27 (11–12) (1985) 908–912.
[111] K. Narita, M. Enokizono, Effect of nickel and manganese addition on ductility and magnetic properties of 6.5% silicon-iron alloy, IEEE Trans. Magn. 14 (4) (1978) 258–262.
[112] Y. Houbaert, R. Colas, J. Barros, D. Ruiz, R. Vandenberghe, M. De Wulf, T. Ros-Yañez, Advances on the characterization of high-silicon steel for electrical applications produced by thermomechanical and dipping-annealing treatment, in: T. Chandra, J.M. Torralba, T. Sakai (Eds.), Thermec'2003, Pts 1-52003, pp. 1145–1150.
[113] T. Ros-Yañez, Y. Houbaert, O. Fischer, J. Schneider, Production of high silicon steel for electrical applications by thermomechanical processing, J. Mater. Process. Technol. 141 (1) (2003) 132–137.
[114] T. Ros-Yañez, Y. Houbaert, O. Fischer, J. Schneider, Thermomechanical processing of high Si-steel (up to 6.3% Si), IEEE Trans. Magn. 37 (4) (2001) 2321–2324.
[115] T. Ros-Yañez, Y. Houbaert, O. Fischer, J. Schneider, Experimental thermo-mechanical processing of high Si-steels (up to 6.5%Si), in: V.G. Baryakhtar (Ed.), European Magnetic Materials and Applications2001, pp. 773–776.
[116] T. Ros-Yanez, D. Ruiz, J. Barros, Y. Houbaert, Advances in the production of high-silicon electrical steel by thermomechanical processing and by immersion and diffusion annealing, J. Alloy. Compd. 369 (1–2) (2004) 125–130.
[117] D. Ruiz, T. Ros-Yanez, R.E. Vandenberghe, E. De Grave, M. De Wulf, Y. Houbaert, Magnetic properties of high Si steel with variable ordering obtained through thermomechanical processing, J. Appl. Phys. 93 (10) (2003) 7112–7114.
[118] X.S. Fang, Y.F. Liang, F. Ye, J.P. Lin, Cold rolled Fe-6.5 wt. % Si alloy foils with high magnetic induction, J. Appl. Phys. 111(9) (2012) 094913.
[119] Y.F. Liang, J.P. Lin, F. Ye, Y.L. Wang, G.L. Chen, Effect of ordering on cold workability of Fe-6.5wt.%Si alloy, in: S.M. Howard (Ed.), Epd Congress 2009, Proceedings, Minerals, Metals & Materials Soc, Warrendale, 2009, pp. 669–674.
[120] Y.F. Liang, F. Ye, J.P. Lin, Y.L. Wang, G.L. Chen, Effect of annealing temperature on magnetic properties of cold rolled high silicon steel thin sheet, J. Alloy. Compd. 491 (1–2) (2010) 268–270.
[121] J.-S. Shin, Z.-H. Lee, T.-D. Lee, E.J. Lavernia, The effect of casting method and heat treating condition on cold workability of high-Si electrical steel, Scr. Mater. 45 (6) (2001) 725–731.
[122] C.-S. Li, C.-L. Yang, G.-J. Cai, Q.-W. Wang, Ordered phases and microhardness of Fe–6.5%Si steel sheet after hot rolling and annealing, Mater. Sci. Eng. A 650 (2016) 84–92.
[123] R. Li, Q. Shen, L. Zhang, T. Zhang, Magnetic properties of high silicon iron sheet fabricated by direct powder rolling, J. Magn. Magn. Mater. 281 (2–3) (2004) 135–139.
[124] S. Wang, Y.M. Jiang, Y.F. Liang, F. Ye, J.P. Lin, Magnetic properties and core loss behavior of Fe-6.5wt.% Si ribbons prepared by melt spinning, Adv. Mater. Sci. Eng. (2015, 2015,) 410830.
[125] H.-Z. Li, H.-T. Liu, Z.-Y. Liu, H.-H. Lu, H.-Y. Song, G.-D. Wang, Characterization of microstructure, texture and magnetic properties in twin-roll casting high silicon non-oriented electrical steel, Mater. Charact. 88 (2014) 1–6.
[126] H.-T. Liu, S.-J. Yao, Y. Sun, F. Gao, H.-Y. Song, G.-H. Liu, L. Li, D.-Q. Geng, Z.-Y. Liu, G.-D. Wang, Evolution of microstructure, texture and inhibitor along the processing route for grain-oriented electrical steels using strip casting, Mater. Charact. 106 (2015) 273–282.
[127] H.-T. Liu, H.-L. Li, H. Wang, Y. Liu, F. Gao, L.-Z. An, S.-Q. Zhao, Z.-Y. Liu, G.-D. Wang, Effects of initial microstructure and texture on microstructure, texture evolution and magnetic properties of non-oriented electrical steel, J. Magn. Magn. Mater. 406 (2016) 149–158.
[128] X. Lu, F. Fang, Y.X. Zhang, Y. Wang, G. Yuan, Y.B. Xu, G.M. Cao, R.D.K. Misra,

G.D. Wang, Evolution of microstructure and texture in grain-oriented 6.5%Si steel processed by strip-casting, Mater. Charact. 126 (2017) 125–134.
[129] Y. Wang, Y.-B. Xu, Y.-X. Zhang, F. Fang, X. Lu, H.-T. Liu, G.-D. Wang, Development of microstructure and texture in strip casting grain oriented silicon steel, J. Magn. Magn. Mater. 379 (2015) 161–166.
[130] Y. Wang, Y.-B. Xu, Y.-X. Zhang, F. Fang, X. Lu, R.D.K. Misra, G.-D. Wang, Effect of annealing after strip casting on texture development in grain oriented silicon steel produced by twin roll casting, Mater. Charact. 107 (2015) 79–84.
[131] Y. Zhang, Y. Xu, H. Liu, C. Li, G. Cao, Z. Liu, G. Wang, Microstructure, texture and magnetic properties of strip-cast 1.3% Si non-oriented electrical steels, J. Magn. Magn. Mater. 324 (20) (2012) 3328–3333.
[132] H.-Y. Song, H.-T. Liu, H.-H. Lu, L.-Z. An, B.-G. Zhang, W.-Q. Liu, G.-M. Cao, L. Cheng-Gang, Z.-Y. Liu, G.-D. Wang, Fabrication of grain-oriented silicon steel by a novel way: strip casting process, Mater. Lett. 137 (2014) 475–478.
[133] H.D. Fu, Z.H. Zhang, X.S. Wu, J.X. Xie, Effects of boron on microstructure and mechanical properties of Fe-6.5 wt.%Si alloy fabricated by directional solidification, Intermetallics 35 (2013) 67–72.
[134] Z.L. Zheng, F. Ye, Y.F. Liang, X.F. Ding, J.P. Lin, G.L. Chen, Formation of columnar-grained structures in directionally solidified Fe-6.5wt.%Si alloy, Intermetallics 19 (2) (2011) 165–168.
[135] Y. Takada, M. Abe, S. Masuda, J. Inagaki, Commercial scale production of Fe-6.5wt.%Si sheet and its magnetic properties, J. Appl. Phys. 64 (10) (1988) 5367–5369.
[136] T. Yamaji, M. Abe, Y. Takada, K. Okada, T. Hiratani, Magnetic properties and workability of 6.5% silicon steel sheet manufactured in continuous CVD siliconizing line, J. Magn. Magn. Mater. 133 (1–3) (1994) 187–189.
[137] W.-J. Park, P068 Health effects after exposure to accidental release of silicon tetrachloride and trichlorosilane, Occup. Environ. Med. 73 (Suppl. 1) (2016) A143–A145.
[138] K.W. Kizer, L.G. Garb, C.H. Hine, Health effects of silicon tetrachloride: report of an urban accident, J. Occup. Environ. Med. 26 (1) (1984) 33–36.
[139] A.E. Cha, Solar Firms Leave Waste Behind in China, Washington Post, 2008.
[140] T. Ros-Yañez, Y. Houbaert, V. Gómez Rodríguez, High-silicon steel produced by hot dipping and diffusion annealing, J. Appl. Phys. 91 (10) (2002) 7857–7859.
[141] X.D. He, X. Li, Y. Sun, Microstructure and magnetic properties of high silicon electrical steel produced by electron beam physical vapor deposition, J. Magn. Magn. Mater. 320 (3–4) (2008) 217–221.
[142] G. Tian, X. Bi, Fabrication and magnetic properties of Fe–6.5% Si alloys by magnetron sputtering method, J. Alloy. Compd. 502 (1) (2010) 1–4.
[143] G.C. Eadie, Continuous spray forming of electrotechnical steel strip, J. Magn. Magn. Mater. 112 (1–3) (1992) 177–178.
[144] C. Bolfarini, M.C.A. Silva, A.M. Jorge Jr, C.S. Kiminami, W.J. Botta, Magnetic properties of spray-formed Fe-6.5%Si and Fe-6.5%Si-1.0%Al after rolling and heat treatment, J. Magn. Magn. Mater. 320 (20) (2008) e653–e656.
[145] A.H. Kasama, C. Bolfarini, C.S. Kiminami, W.J. Botta Filho, Magnetic properties evaluation of spray formed and rolled Fe-6.5 wt.% Si-1.0 wt.% Al alloy, Mater. Sci. Eng.: A (2007) 449375–451377.
[146] R. Machado, A.H. Kasama, A.M. Jorge, C.S. Kiminami, W.J.B. Fo, C. Bolfarini, Evolution of the texture of spray-formed Fe-6.5 wt.% Si-1.0 wt.% Al alloy during warm-rolling, Mater. Sci. Eng. A Struct. Mater. Prop. Microstruct. Process. 449 (2007) 854–857.
[147] R.D. Cava, D.P. Oliveira, T. Yonamine, J.J.A. Moreira, W.J. Botta, C.S. Kiminami, C. Bolfarini, Microstructural characterization of high-silicon iron alloys produced by spray forming and co-injection of Si particles, J. Alloys Compd. 509 (2011) S254–S259.
[148] D. Cava, W.J. Botta, C.S. Kiminami, M. Olzon-Dionysio, S.D. Souza, A.M. Jorge, C. Bolfarini, Ordered phases and texture in spray-formed Fe-5 wt%Si, J. Alloys Compd. 509 (2011) S260–S264.
[149] M.C.A. Silva, C. Bolfarini, C.S. Kiminami, Microstructure and magnetic properties of Fe-6.5wt%Si alloy obtained by spray forming process, Mater. Sci. Forum (2005) 498111–499118.
[150] F.E. Luborsky, J.J. Becker, P.G. Frischmann, L.A. Johnson, Potential of amorphous alloys for application in magnetic devices, J. Appl. Phys. 49 (3) (1978) 1769–1774.
[151] H. Warlimont, R. Boll, Applications of amorphous soft magnetic-materials, J. Magnet. Magn. Mater. 26 (1–3) (1982) 97–105.
[152] A. Makino, T. Hatanai, A. Inoue, T. Masumoto, Nanocrystalline soft magnetic Fe-M-B (M = Zr, Hf, Nb) alloys and their applications, Mater. Sci. Eng. A Struct. Mater. Prop. Microstruct. Process. 226 (1997) 594–602.
[153] 400 Hz Electrical Systems. http://www.aerospaceweb.org/question/electronics/q0219.shtml, (accessed 11/28/2018).
[154] N. Doerry, K. McCoy, Next generation integrated power system: NGIPS technology development roadmap, Naval Sea Systems Command Washington DC, 2007.
[155] R. Hasegawa, Present status of amorphous soft magnetic alloys, J. Magn. Magn. Mater. 215 (2000) 240–245.
[156] L. Solero, A. Lidozzi, J.A. Pomilio, Design of multiple-input power converter for hybrid vehicles, IEEE Trans. Power Electr. 20 (5) (2005) 1007–1016.
[157] C. Heck, Magnetic Materials and their Applications, Elsevier, 2013.
[158] B.G. You, J.S. Kim, B.K. Lee, G.B. Choi, D.W. Yoo, Optimization of powder core inductors of buck-boost converters for Hybrid Electric Vehicles, 2009 IEEE Vehicle Power and Propulsion Conference, 2009, pp. 730–735.
[159] B.J. Lyons, J.G. Hayes, M.G. Egan, Experimental Investigation of Iron-based Amorphous Metal and 6.5% Silicon Steel for High-Current Inductors in Low-Medium Frequency DC-DC Converters, 2007 IEEE Industry Applications Annual Meeting, 2007, pp. 1781–1786.
[160] Magnetic Powder Cores. http://www.mhw-intl.com/assets/CSC/CSC_Catalog.pdf, 11/28/2018).
[161] XFlux® Cores. (accessed 11/28/2018).
[162] Fluxsan. https://www.micrometalsarnoldpowdercores.com/products/materials/fluxsan, (accessed 11/28/2018).
[163] Alloy Powder Core Series Introduction. http://fericor.com/uploads/fericor/public/document/67- sendust_fesi_cores_catalogue_sl.pdf, (accessed 11/28/2018).
[164] M.S. Rylko, K.J. Hartnett, J.G. Hayes, M.G. Egan, Magnetic Material Selection for High Power High Frequency Inductors in DC-DC Converters, 2009 Twenty-Fourth Annual IEEE Applied Power Electronics Conference and Exposition, 2009, pp. 2043–2049.
[165] Y. Tanaka, Y. Takada, M. Abe, S. Masuda, Magnetic-properties Of 6.5-percent Si-Fe sheet and its applications, J. Magn. Magn. Mater. 83 (1–3) (1990) 375–376.
[166] M. Mochizuki, S. Hibino, F. Ishibashi, Application of 6.5-percent silicon steel sheet to induction-motor and its magnetic-properties, Electr. Mach. Power Syst. 22 (1) (1994) 17–29.
[167] R. Kolano, K. Krykowski, A. Kolano-Burian, M. Polak, J. Szynowski, P. Zackiewicz, Amorphous soft magnetic materials for the stator of a novel high-speed PMBLDC motor, IEEE Trans. Magn. 49 (4) (2013) 1367–1371.
[168] R. Hasegawa, Advances in amorphous and nanocrystalline magnetic materials, J. Magn. Magn. Mater. 304 (2) (2006) 187–191.
[169] J.L. McCrea, G. Palumbo, G.D. Hibbard, U. Erb, Properties and applications for electrodeposited nanocrystalline Fe-Ni alloys, Rev. Adv. Mater. Sci. 5 (3) (2003) 252–258.
[170] P.T. Squire, D. Atkinson, M.R.J. Gibbs, S. Atalay, Amorphous wires and their applications, J. Magn. Magn. Mater. 132 (1–3) (1994) 10–21.
[171] M.H. Phan, H.X. Peng, Giant magnetoimpedance materials: fundamentals and applications, Prog. Mater Sci. 53 (2) (2008) 323–420.
[172] K. Mohri, Application of amorphous magnetic wires to computer peripherals, Mater. Sci. Eng. A Struct. Mater. Prop. Microstruct. Process. 185 (1–2) (1994) 141–146.
[173] R. Hasegawa, Applications of amorphous magnetic alloys, Mater. Sci. Eng. A Struct. Mater. Prop. Microstruct. Process. 375 (2004) 90–97.
[174] P. Marin, A. Hernando, Applications of amorphous and nanocrystalline magnetic materials, J. Magn. Magn. Mater. 215 (2000) 729–734.
[175] B.V. Molotilov, V.V. Sadchikov, Amorphous soft magnetic-materials and their application, J. Magn. Magn. Mater. 112 (1–3) (1992) 253–257.
[176] R. Hasegawa, Applications of amorphous magnetic alloys in electronic devices, J. Non-Cryst. Solids 287 (1–3) (2001) 405–412.
[177] C. Miclea, C. Tanasoiu, C.F. Miclea, A. Gheorghiu, V. Tanasoiu, Soft ferrite materials for magnetic temperature transducers and applications, J. Magn. Magn. Mater. 290 (2005) 1506–1509.
[178] .A. DiMarzio, S.A. Oliver, S.W. McKnight, Apparatus and method for measuring instantaneous power using a magneto-optic Kerr effect sensor, Google Patents, 1999.
[179] P. Ripka, Sensors based on bulk soft magnetic materials: advances and challenges, J. Magn. Magn. Mater. 320 (20) (2008) 2466–2473.
[180] J.A. Bas, J.A. Calero, M.J. Dougan, Sintered soft magnetic materials. Properties and applications, J. Magn. Magn. Mater. 254–255 (2003) 391–398.
[181] G. Stojanovic, M. Damnjanovic, V. Desnica, L. Zivanov, R. Raghavendra, P. Bellew, N. Mcloughlin, High-performance zig-zag and in ferrite meander inductors embedded material, J. Magn. Magn. Mater. 297 (2) (2006) 76–83.
[182] Y. Yoshizawa, K. Yamauchi, T. Yamane, H. Sugihara, Common-mode choke cores using the new fe-based alloys composed of ultrafine grain-structure, J. Appl. Phys. 64 (10) (1988) 6047–6049.
[183] M. Pardavi-Horvath, Microwave applications of soft ferrites, J. Magn. Magn. Mater. 215 (2000) 171–183.
[184] R. Boll, H. Warlimont, Applications of amorphous magnetic-materials in electronics, IEEE Trans. Magn. 17 (6) (1981) 3053–3058.
[185] J.P. Liu, E. Fullerton, O. Gutfleisch, D.J. Sellmyer, Nanoscale magnetic materials and applications, Springer, 2009.
[186] G. Ott, J. Wrba, R. Lucke, Recent developments of Mn-Zn ferrites for high permeability applications, J. Magn. Magn. Mater. 254 (2003) 535–537.
[187] R. West, Common mode inductor material selection, in: Proceedings: Electrical Electronics Insulation Conference and Electrical Manufacturing & Coil Winding Conference, 1995, pp. 489–495.
[188] M. Kącki, M.S. Rylko, J.G. Hayes, C.R. Sullivan, Magnetic material selection for EMI filters, IEEE Energy Convers. Congress Exposition (ECCE) 2017 (2017) 2350–2356.
[189] Y. Maillet, R. Lai, S. Wang, F. Wang, R. Burgos, D. Boroyevich, High-density EMI filter design for DC-fed motor drives, IEEE Trans. Power Electr. 25 (5) (2010) 1163–1172.
[190] M. Sugimoto, The past, present, and future of ferrites, J. Am. Ceram. Soc. 82 (2) (1999) 269–280.
[191] L.A. Dobrzański, M. Drak, B. Ziębowicz, New possibilities of composite materials application—Materials of specific magnetic properties, J. Mater. Process. Technol. 191 (1) (2007) 352–355.
[192] I.H. Oh, M. Rayabhari, Single-stage digital power converter for driving LEDs, Google Patents, 2006.
[193] A. Inoue, N. Nishiyama, New bulk metallic glasses for applications as magnetic-sensing, chemical, and structural materials, MRS Bull. 32 (8) (2007) 651–658.
[194] V. Zaspalis, V. Tsakaloudi, E. Papazoglou, M. Kolenbrander, R. Guenther, P. Van der Valk, Development of a new MnZn-ferrite soft magnetic material for high temperature power applications, J. Electroceram. 13 (1–3) (2004) 585–591.
[195] C.H. Smith, Applications of amorphous magnetic-materials at very-high magnetization rates (Invited), J. Appl. Phys. 67 (9) (1990) 5556–5562.
[196] G. Herzer, H.R. Hilzinger, Recent developments in soft magnetic-materials, Phys.

Scripta T 24 (1988) 22–28.
[197] C. Suryanarayana, Nanocrystalline materials, Int. Mater. Rev. 40 (2) (1995) 41–64.
[198] G. Herzer, M. Vazquez, M. Knobel, A. Zhukov, T. Reininger, H.A. Davies, R. Grossinger, J.L.S. Li, Round table discussion: present and future applications of nanocrystalline magnetic materials, J. Magn. Magn. Mater. 294 (2) (2005) 252–266.
[199] C. Suryanarayana, C.C. Koch, Nanocrystalline materials – Current research and future directions, Hyperfine Interact. 130 (1–4) (2000) 5–44.
[200] A. Makino, Nanocrystalline Soft Magnetic Fe-Si-B-P-Cu Alloys With High B of 1.8–1.9T Contributable to Energy Saving, IEEE Trans. Mag. 48 (4) (2012) 1331–1335.
[201] A.D. Setyawan, K. Takenaka, P. Sharma, M. Nishijima, N. Nishiyama, A. Makino, Magnetic properties of 120-mm wide ribbons of high B s and low core-loss NANOMET ® alloy, J. Appl. Phys. 117 (17) (2015).
[202] T.M. Heil, K.J. Wahl, A.C. Lewis, J.D. Mattison, M.A. Willard, Nanocrystalline soft magnetic ribbons with high relative strain at fracture, Appl. Phys. Lett. 90 (21) (2007).
[203] J. Turanová, J. Marcin, J. Ková, D. Janikovi, P. vec, I. korvánek, Magnetic and mechanical properties of nanocrystalline fe-ni-nb-b alloys, J. Phys. Conf. Seri. 144 (1) (2009).